Differential activation of P-TEFb complexes in the development of cardiomyocyte hypertrophy following activation of distinct GPCRs

Ryan D. Martin[a], Yalin Sun[a], Sarah MacKinnon[a], Luca Cuccia[a], Viviane Pagé[a], Terence E. Hébert[a#], Jason C. Tanny[a#]

[a]Department of Pharmacology and Therapeutics, McGill University, Montréal, Québec, Canada

Running Head: Receptor-specific activation of Brd4 in cardiomyocytes

#Address correspondence to Dr. Jason C. Tanny, jason.tanny@mcgill.ca or Dr. Terence E. Hébert, terence.hebert@mcgill.ca.

Word count for abstract: 200

Word count for Materials and Methods: 2079

Word count for rest of text: 6237

Abstract

Pathological cardiac hypertrophy is driven by neurohormonal activation of specific G protein-coupled receptors (GPCRs) in cardiomyocytes and is accompanied by large-scale changes in cardiomyocyte gene expression. These transcriptional changes require activity of positive transcription elongation factor b (P-TEFb), which is recruited to target genes by the bromodomain protein Brd4 or the *S*uper *E*longation *C*omplex (SEC). Here we describe GPCR-specific regulation of these P-TEFb complexes and a novel mechanism for activating Brd4 in primary neonatal rat cardiomyocytes. The SEC was required for the hypertrophic response downstream of either the α_1-adrenergic receptor (α_1-AR) or the endothelin receptor (ETR). In contrast, Brd4 inhibition selectively impaired the α_1-AR response. This was corroborated by the finding that activation of α_1-AR, but not ETR, increased Brd4 occupancy at promoters and super enhancers of hypertrophic genes. Transcriptome analysis demonstrated that activation of both receptors initiated similar gene expression programs, but that Brd4 inhibition attenuated hypertrophic genes more robustly following α_1-AR activation. Finally, we show that protein kinase A (PKA) is required for α_1-AR stimulation of Brd4 chromatin occupancy. The differential role of the Brd4/P-TEFb complex in response to distinct GPCR pathways has potential clinical implications as therapies targeting this complex are currently being explored for heart failure.

Introduction

The heart undergoes extensive remodelling in response to various mechanical and hormonal stressors during the progression to heart failure following myocardial infarction and/or sustained hypertension (1, 2). This includes hypertrophy of terminally differentiated cardiomyocytes in order to sustain cardiac output (3). While initially adaptive, prolonged

cardiomyocyte hypertrophy leads to cardiomyocyte death, fibrosis and progression to chronic heart failure (4). Cardiomyocyte hypertrophy is initiated in part by neurohormonal activation of G protein-coupled receptors (GPCRs), such as the α_1-adrenergic receptor (α_1-AR), endothelin-1 receptor (ETR), and β-adrenergic (βAR) families (5, 6). Upon ligand binding, GPCRs activate heterotrimeric G proteins comprised of a Gα subunit and the obligate heterodimer Gβγ. Both the α_1-AR and ETR canonically activate Gαq signalling, whereas the β-AR activates Gαs signalling. Cardiac-specific overexpression of Gαq and Gαs isoforms in mice leads to cardiomyopathy phenotypes, including cardiomyocyte hypertrophy (7, 8). The Gα isoforms elicit distinct signalling pathways involving calcium release and cyclic AMP (cAMP) formation respectively, which are capable of activating transcription factors and a gene expression program culminating in cardiomyocyte hypertrophy (9, 10). These pathological gene expression changes also require the coordinated interplay between dynamic alterations in chromatin structure, various master transcription factors and general transcriptional regulators, such as positive transcription elongation factor b (P-TEFb) (9, 11, 12).

P-TEFb, a heterodimer consisting of cyclin-dependent kinase 9 and cyclin T, positively regulates the release of RNA polymerase II (RNAPII) from a promoter proximal paused state into productive elongation. P-TEFb phosphorylates multiple proteins in the RNAPII elongation complex, including the C-terminal repeat domain of RNAPII itself, DRB sensitivity inducing factor (DSIF), and negative elongation factor (NELF) (13). In cardiomyocytes, P-TEFb activity is regulated by Gαq signalling as evidenced by cardiac-specific overexpression of Gαq in mice and ETR activation in primary neonatal rat cardiomyocytes (11). P-TEFb is a critical regulator for cardiomyocyte hypertrophy, with inhibition preventing the gene expression and cell size changes characteristic of cardiomyocyte hypertrophy (11). These transcriptional events require

recruitment of the active P-TEFb complex to chromatin. P-TEFb recruitment is predominantly regulated through interactions with the bromodomain and extra-terminal (BET) protein Brd4 or through interactions with the super elongation complex (SEC) (14, 15).

Like other BET family members (Brd2, Brd3, and testis specific BrdT), Brd4 contains two N-terminal bromodomains, which bind to acetylated lysines on histone proteins leading to recruitment of Brd4 to chromatin, as well as an extra-terminal domain, which interacts with multiple transcriptional regulators (16). Brd4 and BrdT contain an additional domain that interacts with P-TEFb (17). The importance of Brd4 as a regulator of P-TEFb and transcription elongation in cardiomyocyte hypertrophy has been demonstrated using small molecule inhibitors of the BET bromodomain/acetyl lysine interaction such as JQ1 (18-21). JQ1 treatment reduced stress-induced gene expression and cardiomyocyte hypertrophy in primary culture models and in mice subjected to pressure overload via transverse aortic constriction (TAC), a potent inducer of cardiac hypertrophy *in vivo* (18, 21). Brd4 inhibition was also able to partially reverse pre-established signs of heart failure in a mouse model of myocardial infarction and pressure overload (20). These effects are correlated with the loss of Brd4 from super-enhancers and promoters of hypertrophic genes in cardiomyocytes, as well as reduced RNAPII elongation.

Multiple forms of SEC have been found in mammalian cells, comprised of P-TEFb, AF9, ENL, the three ELL family members (ELL1/2/3), EAF1/2, AFF1 and AFF4 (22). The SEC positively regulates release of RNAPII from promoter proximal-pausing to productive elongation (23). Aberrant targeting and activity of the SEC underlies development of various cancers and developmental diseases. For example, mixed lineage leukemia 1 (MLL) is fused to various SEC subunits in certain types of acute leukemias (24) and a germline Aff4 gain-of-function mutation leads to the developmental syndrome CHOPS (*C*ognitive impairment and coarse facies, *H*eart

92 defects, *O*besity, *P*ulmonary involvement and *S*hort stature and skeletal dysplasia) (25).
93 Although RNAPII promoter proximal pausing is dysregulated in cardiac hypertrophy, the role of
94 the SEC in regulating the hypertrophic gene expression program in cardiomyocytes has not been
95 investigated.

96 How diverse signaling pathways involved in cardiac remodelling cooperate to orchestrate
97 the hypertrophic gene expression program *in vivo* remains poorly understood. Although
98 neurohormonal signals induce similar hypertrophic responses in primary cardiomyocytes,
99 distinct signalling pathways are initiated through activation of their cognate GPCRs (26). Such
100 effects are generally attributed to differential G protein coupling, however receptor-specific
101 differences in downstream effector protein activation of the same Gα subunit have also been
102 demonstrated (27). The coordination between these signalling pathways, and the fact that each
103 activates a unique combination of transcription factors, suggests that there may be differences in
104 how they regulate gene expression. However, comparison of changes in gene expression have
105 only been assessed for a limited repertoire of genes (28, 29). How different receptors alter global
106 transcriptional regulation has not been systematically compared. Such differences may have
107 important therapeutic implications for treating patients with heart disease stemming from varied
108 clinical origins.

109 In this study we focused on the differential impact of cardiomyocyte GPCR signalling
110 pathways on mechanisms regulating transcription. We investigated the role of P-TEFb and its
111 interacting partners, Brd4 and SEC, in cardiomyocyte hypertrophy caused by activation of either
112 of two GPCRs, the α_1-AR or ETR. These receptors are canonically thought to elicit their
113 hypertrophic responses through Gαq activation, with both receptors also able to activate
114 additional Gα subunits which has not been thoroughly assessed. We found that P-TEFb activity

and the SEC are required for cardiomyocyte hypertrophy induced by activation of either GPCR. However, only the α_1-AR response was attenuated by Brd4 inhibition. Transcriptome analysis after Brd4 inhibition indicated attenuation of α_1-AR upregulated genes that were enriched for pathways involved in the pathophysiology of cardiomyocyte hypertrophy. Brd4 chromatin occupancy at promoters and super enhancers of hypertrophic genes was specifically induced by α_1-AR activation, an effect that was dependent on the activity of PKA. Lastly, we demonstrated that the hypertrophic response downstream of another receptor known to signal through PKA, the β-AR, was also attenuated by Brd4 inhibition. Our study suggests receptor-specific regulation of P-TEFb function and expands the currently known cellular repertoire of protein kinases capable of regulating Brd4 function. Further, our findings suggest that the clinical efficacy of BET inhibitors for heart failure may depend on patients' specific neurohormonal signalling patterns.

Results

Evidence for receptor-specific P-TEFb regulation in cardiomyocyte hypertrophy

We first revisited the requirement of P-TEFb activity for the hypertrophic response in primary neonatal rat cardiomyocytes (NRCMs). Previous experiments used the ATP analog 5,6-dichlorobenzimidazone-1-β-D-ribofuranoside (DRB), a cyclin-dependent kinase inhibitor that affects Cdk9, to implicate P-TEFb activity in the hypertrophic response (11). To confirm these results, we repeated this experiment using iCdk9, a Cdk9 inhibitor that is ~1000 times more potent and ~100 times more selective than DRB (30). Following 24 h treatment, agonists for the ETR (endothelin-1; ET-1) or α_1-AR (phenylephrine; PE) increased cardiomyocyte surface area by 35-40% relative to control, as assessed by analysis of α_2-actinin immunostaining using high-

content microscopy (Figures 1A and 1B). Simultaneous treatment with 0.2 μM iCdk9 completely abolished the increase in cardiomyocyte size elicited by either agonist, confirming a stringent requirement for P-TEFb activity in cardiomyocyte hypertrophy (Figures 1A and 1B).

To further characterize P-TEFb function in the hypertrophic response, we assessed the roles of the SEC and Brd4, two key P-TEFb-interacting proteins (31). To perturb the P-TEFb/SEC interaction, we used KL-2, which prevents the interaction between the cyclin T component of P-TEFb and the SEC scaffolding subunit Aff4 (32). KL-2 treatment blocked the increase in cell size in response to both ETR and α_1-AR activation, similar to the effect of Cdk9 inhibition (Figures 2A and 2B). To determine whether disruption of the P-TEFb/SEC interaction also affected the expression of hypertrophic genes, we monitored changes in mRNA levels for established hypertrophy marker genes Nppa, Nppb, and Serpine1 using RT-qPCR. Whereas mRNA levels for these genes were robustly increased in response to activation of either receptor, induction of Nppb and Nppa was blocked by KL-2 co-treatment (Figure 2C). Interestingly, Serpine1 induction was unaffected by KL-2 treatment indicating a gene-specific aspect to SEC function. To confirm the observed effect was due to disruption of SEC function, we next reduced Aff4 levels using siRNA and verified knockdown by RT-qPCR (Figure 2D). Similar to KL-2 treatment, knockdown of Aff4 blocked the increase in cell size following activation of either receptor (Figure 2E).

We next tested the role of Brd4 using the pan-BET small-molecule inhibitor JQ1. JQ1 targets the BET family bromodomains, acting to competitively inhibit their interaction with acetylated lysine residues (33). Interestingly, BET inhibition attenuated the hypertrophic response in a receptor-specific manner: the response to α_1-AR activation was decreased, whereas there was no effect on ETR-mediated increase in cell size (Figures 3A and 3B). We also

observed that JQ1 treatment more strongly reduced expression of hypertrophic marker genes in cells stimulated with the α_1-AR agonist compared to cells stimulated with an ETR agonist (Figure 3C). One possible explanation for the receptor-specific effect of JQ1 is that the dose of ET-1 used to drive hypertrophy was sufficiently high to overcome JQ1 inhibition. To address this, we tested the effect of JQ1 on the ET-1-driven hypertrophic response over a wide range of ET-1 doses. The ET-1 response was insensitive to JQ1 at all doses tested (Figure 4). Thus, receptor-specific differences in JQ1 sensitivity likely reflect intrinsic differences in the respective GPCR signalling outcomes. These data suggest that the SEC is generally required for P-TEFb function in the hypertrophic response, whereas the P-TEFb/Brd4 complex mediates receptor-specific functions.

As JQ1 inhibits all members of the BET family of bromodomain proteins, we confirmed the effects on hypertrophy were mediated by Brd4 and not Brd2 and/or Brd3. Brd2, Brd3, and Brd4 were individually depleted in NRCMs using siRNA (Figure 5A). Hypertrophic responses were then induced through activation of the α_1-AR or ETR. Brd2 and Brd3 knockdown reduced the basal size of NRCMs relative to control siRNA (Figures 5B), but the response following activation of either receptor was comparable to that observed with control siRNA (Figure 5C). In contrast, Brd4 knockdown recapitulated the effects observed with JQ1 in that it attenuated the response to α_1-AR activation but did not affect ETR-mediated hypertrophy (Figures 5B and 5C). These data argue that Brd4 inhibition accounts for the receptor-specific effects of JQ1 on cardiomyocyte hypertrophy.

To gain further insight into how Brd4 function is differentially affected by distinct GPCR signalling pathways, we assessed gene-specific Brd4 localization to chromatin using chromatin immunoprecipitation coupled to qPCR (ChIP-qPCR). ChIP was performed using an antibody

recognizing endogenous Brd4 and was quantified by qPCR using primer pairs near the transcription start sites of Nppb, Nppa, and Serpine1. Occupancy at previously defined super enhancers for Nppb and Serpine1 in cardiomyocytes was also assessed (19). At all genomic loci tested, 24 h α_1-AR activation increased Brd4 chromatin occupancy compared to vehicle treatment (Figure 6A). We observed no change in Brd4 occupancy compared to vehicle following ETR treatment, despite the fact that mRNA levels for the same genes were similarly induced by PE and ET-1 (Figures 2C and 3C). The effects on Brd4 occupancy were not simply a reflection of altered Brd4 protein levels, as immunoblots performed on cell extracts from NRCMs treated with PE or ET-1 revealed slight decreases in expression compared to vehicle controls (Figures 6B and 6C). This suggests that signalling through α_1-AR, but not ETR, triggers recruitment of Brd4, making gene expression changes downstream of this receptor more sensitive to Brd4 inhibition by JQ1.

RNA-seq reveals differences in GPCR-dependent signalling between hypertrophic agonists

To comprehensively profile receptor-specific effects on cardiomyocyte hypertrophy, we performed RNA-seq on NRCMs following activation of either receptor for 24 h in the presence or absence of JQ1. When comparing agonist versus vehicle conditions, we observed robust gene expression changes [$\log_2$(Fold Change) > ±1 and p-value < 0.05] for hundreds of genes following ETR (209 upregulated, 192 downregulated) or α_1-AR activation (269 upregulated, 279 downregulated). The genes regulated by either receptor overlapped significantly, although there were more genes uniquely regulated by α_1-AR activation than by ET-1 activation (Figures 7A and 7B). The combined effect of receptor agonists and JQ1 on differential expression was visualized by performing K-means clustering (Figures 7C and 7D). This analysis identified three

major gene clusters that were similarly regulated by agonist and JQ1: one in which genes were repressed by agonist in the presence or absence of JQ1 (cluster 1), one in which genes were activated by agonist and attenuated by JQ1 (cluster 2), and one in which genes were activated by agonist in the presence or absence of JQ1 (cluster 3). The observation that the primary effect of JQ1 was to dampen expression of genes regulated by receptor activation aligns with the known roles of Brd4 in recruiting P-TEFb to regulate pause-release and activate transcription (15), and is consistent with the effect of JQ1 on cardiac stress-induced genes previously characterized (20).

We focused on groups of genes for which increased expression caused by activation of either receptor was attenuated by JQ1 [$\log_2$(Fold Change) < -0.5 compared to agonist alone; p-value < 0.05]. JQ1 attenuated expression of 107 ETR-induced genes and 155 α_1-AR-induced genes (termed receptor+/JQ1-) (Figure 7E). A majority of the ETR+/JQ1- genes overlapped with α_1-AR+/JQ1- genes (83.2% overlap, 16.8% unique), whereas there was a large number of unique α_1-AR+/JQ1- genes (57.4% overlap, 42.6% unique). Gene ontology term analysis of these gene sets revealed that the terms inflammatory response, defense response, cell adhesion, cardiac muscle tissue growth and heart growth, which correspond to the pathophysiology of cardiomyocyte hypertrophy and align with those previously identified to be affected by JQ1, were significantly enriched among the AR+/JQ1- genes (Figure 7F) (20). In contrast, none of these terms were significantly enriched among ETR+/JQ1- genes, consistent with the selective effect of JQ1 on the α_1-AR response.

Previous studies have identified multiple transcription factors that are required to activate pro-hypertrophic genes in cardiomyocytes (9, 34). Some of these transcription factors have been associated with Brd4 activity in cardiomyocytes, either through motif enrichment in genomic loci with high Brd4 occupancy or various gene set enrichment methods for JQ1-sensitive genes.

The pathway-specific effect of Brd4 inhibition suggests that specific transcription factors may be dependent on Brd4 to activate transcription. We initially focused on those transcription factors that were previously implicated including, NF-κB, GATA4, and the AP-1 subunits Jun and Fos (Figure 7G) (18-20). To determine the effect of JQ1 on these transcription factors, we used Ingenuity Pathway Analysis software (IPA; Qiagen) to predict changes in their activity (Figure 7G). IPA upstream regulator analysis provides a z-score, to indicate the predicted change in activity between the two treatment groups, and a Fisher's exact test p-value, to indicate whether particular upstream regulator's target genes are significantly enriched in the gene expression program. Interestingly, IPA predicted increased activity of these transcription factors following activation of either receptor (positive z-score, agonist/vehicle vs vehicle/vehicle), but activity was specifically attenuated by JQ1 following α_1-AR activation (negative z-score, agonist/JQ1 vs agonist/vehicle) (Figure 7G). This suggests that receptor-specific activation mechanisms for these transcription factors dictate their dependence on Brd4 activity. When we expanded the analysis to include all activated transcription factors a more ubiquitous effect of Brd4 inhibition was observed. We identified 78 transcription factors with enhanced activity following α_1-AR activation of which activity of 39 (50%) were attenuated by co-treatment with JQ1. In contrast, ETR activation was predicted to enhance activity of 50 transcription factors and only eight (16%) were attenuated by JQ1. Thus, although specific transcription factors may function to recruit Brd4 to specific loci, the more ubiquitous effect of Brd4 inhibition on α_1-AR-mediated transcription factor activity suggests that α_1-AR signalling may increase the pool of active Brd4.

Signalling pathway regulating Brd4 recruitment to chromatin involves PKA

We hypothesized that a distinct signalling pathway activated by the α_1-AR determines differential recruitment of Brd4 and inhibitory effect of JQ1 on transcription factor activity. Brd4 is activated following phosphorylation of its phosphorylation dependent interaction domain (PDID). An *in vitro* kinase assay demonstrated that PKA was able to phosphorylate this region, although the functional significance was not determined (35). We have previously demonstrated that α_1-AR, but not ETR activation, led to Gαs-dependent activation of cAMP/PKA signalling in HEK 293 cells (36). We thus hypothesized that PKA, a protein kinase activated by cAMP, regulates the specific effects of α_1-AR signalling on Brd4 in cardiomyocytes.

We confirmed that α_1-AR and not ETR signalling activated PKA in NRCMs. Cardiomyocytes were transduced with a nuclear-localized Förster resonance energy transfer (FRET)-based PKA biosensor (AKAR4-NLS) to monitor PKA activity (37). When phosphorylated, the biosensor undergoes a conformational change that moves the two fluorophores into closer proximity, leading to an increased FRET ratio. Nuclear localization of the AKAR biosensor was confirmed by fluorescence microscopy (Figure 8A). We then generated a dose-response relationship for PKA activity following stimulation with ET-1 and PE. Alprenolol was included in the PE experiments to prevent off-target effects on the β-AR at high concentrations. We observed a dose-dependent increase in FRET, indicating an increase in PKA activity, following 15 min α_1-AR activation. In contrast, no change in activity was observed following 15 min ETR activation (Figure 8B). This demonstrated that the α_1-AR uniquely activates PKA in the nucleus of cardiomyocytes, similar to what we detected in HEK 293 cells (36).

In order to determine if PKA activity downstream of the α_1-AR regulates Brd4 function in cardiomyocytes, we performed ChIP-qPCR after inhibition or activation of PKA. To inhibit

PKA, we used the competitive inhibitor KT5720 (38). As we anticipated that long-term PKA inhibition could cause other changes in cellular physiology that would complicate interpretation of the experiments, we used a treatment time of 1.5 h. We quantified Brd4 localization using primer pairs near the transcription start site of c-Fos and Ctgf as well as previously defined super-enhancer regions of Ctgf (19). Activation of the α_1-AR for 1.5 h enhanced Brd4 occupancy near the transcription start sites of both genes and along the previously defined Ctgf super enhancers, whereas ETR stimulation had no effect (Figures 9A and 9B). These data suggest that the specific effect of α_1-AR signalling on Brd4 chromatin occupancy is maintained at the shorter treatment time. Pre-treatment with KT5720 abrogated the increase in Brd4 occupancy following α_1-AR activation, consistent with a requirement for PKA activity for chromatin recruitment of Brd4 downstream of α_1-AR signalling (Figure 9A and 9B). PKA inhibition also increased the basal occupancy of Brd4 at these sites, perhaps reflecting a repressive function for PKA in unstimulated NRCMs. We also stimulated activation of PKA in NRCMs by increasing intracellular cAMP levels with forskolin and IBMX, an adenylyl cyclase activator and phosphodiesterase inhibitor, respectively (39). Sustained PKA activation (1.5 h) increased Brd4 chromatin association at two of the four genomic loci assessed, reinforcing the key role of PKA in Brd4 activation (Figure 9C).

To test whether a regulatory link between PKA and Brd4 could be detected in response to other GPCRs coupled to Gαs, we examined the role of Brd4 downstream of the β-AR, activation of which is strongly pro-hypertrophic in cardiomyocytes (40). The primary signalling pathway downstream of this receptor in cardiomyocytes (and other cell types as well) involves adenylyl cyclase activation, cAMP production, and increased protein kinase A activity (41). We thus predicted that hypertrophy mediated by the β-AR would also be attenuated by inhibition of Brd4

298 with JQ1. Following 24 h treatment with the agonist isoproterenol, we observed a ~25% increase
299 in surface area which was completely blocked by co-treatment with JQ1 (Figure 9D and 9E).
300 This demonstrates that the observed connection between PKA and Brd4 is not unique to α_1-AR
301 signalling and may reflect a general Gαs-coupled GPCR-dependent pathway for Brd4 activation.
302 Taken together, our results point to PKA and Brd4 as central players underlying receptor-specific
303 gene regulatory mechanisms in hypertrophic cardiomyocytes (Figure 10).
304
305 **Discussion**
306 In this study, we showed that activation of distinct GPCRs in cardiomyocytes can result
307 in hypertrophic responses and gene expression programs that are qualitatively similar, but that
308 operate through different transcriptional regulatory mechanisms. We also identified a novel
309 mechanism regulating Brd4 in the development of cardiomyocyte hypertrophy that expands our
310 understanding of how specific signalling pathways regulate the recruitment of general
311 transcription regulators and that may have relevance in other physiological contexts.
312 Chromatin occupancy of Brd4 undergoes extensive redistribution in order to positively
313 regulate expression of the cardiomyocyte hypertrophic gene program. These changes lead to
314 enhanced Brd4 occupancy on specific super-enhancers and promoter regions. Previous Brd4
315 ChIP-seq experiments have used primary cardiomyocytes treated with PE (in accord with our
316 results), or cardiac tissue isolated from mice subjected to transverse aortic constriction (TAC)
317 (19, 20). The increased genomic loading of Brd4 in heart failure models has been attributed to
318 increases in Brd4 expression (19), similar to proposed mechanisms in various forms of cancer
319 (42-44). In heart failure, increased Brd4 protein expression is thought to occur due to decreased
320 expression of the Brd4 targeting microRNA miR-9 (21, 45). These reports assessed whole

cardiac tissue not enriched for cardiomyocytes or *in vitro* cardiomyocyte studies which reported conflicting evidence regarding changes in Brd4 expression (18, 21). Following 24 h activation of the α1-AR or ETR in cardiomyocytes, we did not observe a significant change in Brd4 protein expression (Figure 6B). Instead, the increased Brd4 recruitment following α_1-AR activation was dependent on cAMP/PKA signalling pathway.

Phosphorylation of Brd4 is critical for its activation and also mediates alterations in its interactome. Brd4 hyperphosphorylation correlates with its oncogenic potential and increased phosphorylation levels lead to development of BET inhibitor resistance in certain types of cancer (46, 47). At present, casein kinase 2 (CK2) is the only protein kinase demonstrated to directly phosphorylate Brd4, although others have been shown to regulate Brd4 activity (35, 46, 48). CK2 phosphorylation sites reside within the PDID domain, where phosphorylation results in a conformational change that unmasks the second bromodomain and enables interactions with acetyl-lysine residues (35). An *in vitro* kinase screen of the PDID domain identified PKA as a potential Brd4 kinase, aligning with the PKA regulatory effect on Brd4 we observed (35). This suggests that in cardiomyocytes, enhanced PKA activity could increase PDID phosphorylation and drive the conformational change required for Brd4 to interact with chromatin. Further work remains to identify the putative phosphorylated sites and elucidate their functional role(s). Conversely, we also observed an increase in basal Brd4 occupancy following PKA inhibition (Figure 9A). Such increased Brd4 occupancy may be related to PKA's known role in regulating histone deacetylases (49). The balance between these two opposing processes regulated by PKA is likely linked to the highly localized nature of PKA signalling through interactions with A-kinase anchoring proteins (AKAPs) (50).

RNA-seq analyses revealed that the transcriptional programs triggered by activation of α_1-AR or ETR were highly overlapping, consistent with the similar hypertrophic response downstream of either receptor. The mechanistic difference between the two pathways was instead linked to the fact that specific groups of genes relevant to the hypertrophic response were differentially sensitive to JQ1 downstream of α_1-AR activation compared to ETR. Previous reports have identified inflammatory pathways enriched in JQ1-attenuated genes using both *in vitro* and *in vivo* models of cardiomyocyte hypertrophy (20). We observed JQ1-selective attenuation of these inflammatory pathways following α_1-AR activation (Figure 7F). We argue that this difference stems from a greater role for Brd4 downstream of α_1-AR, consistent with our Brd4 ChIP results. Such inflammatory responses are characteristic of heart failure, and the production of several cytokines is increased during cardiac remodelling (51, 52). Importantly, inflammation is a driver of cardiomyocyte hypertrophy and inhibition of those pathways prevents the progression of heart failure (53, 54). Although specific pathways were not enriched among genes attenuated by JQ1 follow ETR activation, a large number of genes did exhibit JQ1 sensitivity. We suspect the observed effects are likely due to functions of Brd2 and/or Brd3 in regulating these genes, although further work is required to confirm this.

Further evidence for the effect of JQ1 on the inflammatory response is evident by the negative effect on inflammatory transcription factors such as NF-κB and AP-1 (Figure 7G) (34, 55, 56). We focused on these transcription factors for two reasons: their gene expression signatures were previously identified in JQ1-sensitive, TAC-induced genes, or a causal role in regulating Brd4 recruitment in cardiomyocytes has been identified (18, 19). Importantly, these transcription factors are also directly implicated in driving pathological cardiomyocyte hypertrophy in various *in vitro* and *in vivo* models (57-61). Despite the fact that similar

366 transcription factors were activated downstream of α_1-AR and ETR, JQ1 only attenuated the α_1-
367 AR response. The receptor-specific attenuation of transcription factor activity may be due to
368 distinct signalling mechanisms required for transcription factor activation, creating a differential
369 dependence on Brd4 activity (62-65). However, the greater number of transcription factors
370 attenuated by JQ1 following α_1-AR activation suggests that it leads to an active form of Brd4
371 that more readily binds to chromatin and promotes the activity of transcription factors. Although
372 we predict that PKA activates Brd4 directly, indirect activation through a downstream factor is
373 also possible. Further investigation is required to determine the effects of JQ1 on Brd4's
374 interactome and phosphorylation status following α_1-AR or ETR activation.

375 Receptor-specific activation of Brd4 we identified may have implications for the clinical
376 use of Brd4 inhibitors in cardiovascular disease. Efficacy will be dependent on the specific
377 neurohormonal signalling pathways altered in a particular patient. Specifically, we would expect
378 a negative correlation with a patient's ET-1 levels. Therefore, more extensive characterization of
379 signalling molecules in patients might be important predictors of drug efficacy. Importantly, we
380 expect that Brd4 inhibition will be less effective in severe and/or late stages of heart failure as
381 PKA activity is reduced (41) and levels of endothelin-1 or its precursors (66-68) increases.
382 Chronic infusion of these neurohormones with mice is required to determine how the receptor-
383 specific effects of Brd4 inhibition effects cardiac remodelling. Furthermore, although JQ1 has
384 been demonstrated to reverse established heart failure in mouse TAC and myocardial infarction
385 mouse models (20), we expect JQ1 efficacy would decrease as heart failure progresses.

386 Our finding that JQ1 sensitivity is dependent on activation of PKA signalling raises the
387 question of whether Brd4 inhibition is also an effective therapeutic for other pathologies
388 associated with enhanced PKA signalling. For example, chronic activation of PKA is a hallmark

389 of dopamine-dependent neuronal pathologies such as cocaine addiction and L-DOPA induced
390 dyskinesia (LID) (69, 70). Recent studies have implicated Brd4 in regulating the neuronal
391 transcriptional programs and behavioural effects driven by dopamine signalling in these contexts.
392 Systemic administration of JQ1 reduces reward seeking behaviour in addiction models and
393 prevents LID development in Parkinson's models (71, 72). The correlation between PKA and
394 Brd4 activity in these cases suggests that the regulation of Brd4 chromatin occupancy by PKA
395 might be a common regulatory mechanism for other GPCRs and cell types. Furthermore, certain
396 adrenocortical adenomas are driven by enhanced basal PKA activity due to activating mutations
397 in Gαs or the catalytic subunit of PKA (73, 74). We expect these adenomas would be highly
398 sensitive to Brd4 inhibition, although further work is required to establish the requirement of
399 Brd4 in progression of these cancers.

400 Dysregulated activation and recruitment of P-TEFb is an underlying cause of several
401 diseases and developmental disorders (75). While recruitment of P-TEFb is regulated either by
402 Brd4 or the SEC, little is known about the functional relationship between these two complexes.
403 It has been suggested that these complexes work together to target P-TEFb to different substrates
404 whereas others have shown that Brd4 assists in recruiting the SEC (76, 77). Our results indicate
405 the cooperative nature of these two complexes is dependent on the signalling pathway employed
406 to activate transcriptional responses. Following ETR activation, the SEC alone is sufficient to
407 elicit a gene expression program required for cardiomyocyte hypertrophy, whereas the activation
408 of the Gαs/cAMP/PKA pathway by the α_1-AR leads to an additional dependence on Brd4. This
409 suggests that the SEC form of P-TEFb may have a general transcriptional regulatory role
410 whereas the form associated with Brd4 may have a more restricted signal-responsive role.
411 Further investigation is required to assess whether these complexes have distinct or overlapping

functions in cardiomyocytes. Furthermore, expanding our understanding of how signalling pathways activate these complexes is an important step to improve therapeutic approaches in diseases with dysregulated P-TEFb.

Methods

Primary neonatal rat cardiomyocyte isolation, tissue culture, transfection and treatments

Unless otherwise stated, all reagents were obtained from Sigma. Primary rat cardiomyocytes were isolated from 1-3 day old Sprague-Dawley rats (Charles River Laboratories, St-Constant, Quebec) as previously described with minor modifications (78). Following isolation, cardiomyocytes were seeded at a density of 40 000 cells/cm^2 on tissue culture dishes coated with 0.1% gelatin and 10 μg/mL fibronectin in DMEM low glucose (Wisent) supplemented with 7% FBS (Wisent) (v/v), 1% (v/v) penicillin/streptomycin (P/S), and 10 μM cytosine-β-d-arabinoside (MP Biomedicals). After 24 h, plates were washed twice with DMEM low glucose and media changed to cardiomyocyte maintenance media (DMEM low glucose, 1% (v/v) insulin/selenium/transferrin (Wisent), and 1% (v/v) P/S) with 10 μM cytosine-β-d-arabinoside. Twenty-four hours later, media was replaced with fresh cardiomyocyte maintenance media and experiments were initiated 24h later. Cardiomyocytes were maintained at 37°C with 5% CO_2 and typical cultures contained >90% cardiomyocytes. Cardiomyocytes were treated with endothelin-1 (Bachem), phenylephrine, iCdk9 (Novartis), KL-2 (ProbeChem Biochemicals), JQ1, alprenolol, KT5720, forskolin, 3-isobutyl-1-methylxanthine (IBMX), or isoproterenol.

For small interfering RNA (siRNA) transfection (siGENOME SMARTPool, Horizon Discover), cardiomyocytes were pelleted at 400 g for 5 min at 4°C after isolation, resuspended in

DMEM low glucose supplemented with 2.5% (v/v) FBS and plated at a density of 60 000 cells/cm^2. Cardiomyocytes were transfected with 50 nM siRNA for the specified target gene with Lipofectamine 2000 (Invitrogen) according to the manufacturer's instructions. After 5h incubation, the media was replaced with DMEM low glucose supplemented with 7% FBS (v/v), 1% (v/v) penicillin/streptomycin (P/S), and 10 μM cytosine-β-d-arabinoside and cultured as previously described.

Immunofluorescence and measurement of cell area

Cardiomyocytes were plated in 96-well plates and cultured as described. Following indicated treatment, cells were fixed with methanol for 5 min at -20°C, permeabilized with 0.2% Triton X-100 (v/v) in PBS for 5 min at room temperature and blocked with 10% horse serum (Wisent) in PBS for 1 h at room temperature. Primary anti-α_2-actinin antibody (Sigma, A7811; 1/200) in 10% horse serum/PBS was incubated with cardiomyocytes overnight at 4°C. The following day, the fixed cardiomyocytes were incubated with anti-mouse Alexa Fluor 488 secondary antibody (Invitrogen, A-11029; 1/500) in 10% horse serum/PBS for 1 h at room temperature and 10 min with Hoechst dye (Invitrogen) (1 μg/μL) in PBS at room temperature. Stained cardiomyocytes were imaged with an Operetta high-content screening system (PerkinElmer) with 20X magnification and analyzed with Columbus Image Analysis System (PerkinElmer). Hoechst dye was excited with a 360-400 nm filter and emissions detected at 410-480 nm and Alexa 488 was excited with a 460-490 nm filter and emissions detected at 500-550 nm. The average of two technical replicates was taken for all treatments.

AKAR4-NLS AAV transduction and FRET experiments

The AKAR4-NLS construct was a gift from Dr. Jin Zhang (UCSD) and the pAAV-CAG-GFP was a gift from Dr. Karel Svoboda (Addgene plasmid #28014) (79, 80). To generate the AKAR4-NLS biosensor for adeno-associated virus (AAV) production, AKAR4-NLS biosensor was excised and cloned into the pAAV backbone using BamHI and EcoRI (New England Biolabs) at the 5' and 3' end, respectively. For AAV production, HEK 293T cells were maintained in DMEM high glucose supplemented with 10% (v/v) FBS and 1% (v/v) P/S in a controlled environment of 37°C and 5% CO_2. Adeno-associated viruses were produced as previously described (81).

Twenty-four hours after plating cardiomyocytes, media was changed to cardiomyocyte maintenance media with AAV9-packaged AKAR4-NLS biosensor at a multiplicity of infection (MOI) of 5000. Following 24 h transduction, media was changed to cardiomyocyte maintenance media and changed every 24 h until experiment. After 48 h incubation, cardiomyocyte maintenance media was removed and cells were washed with Krebs solution (146 mM NaCl, 4.2 mM KCl, 0.5 mM $MgCl_2$, 1 mM $CaCl_2$, 10 mM HEPES pH 7.4, 1 g/L glucose) and incubated for 1 h at 37°C with 5% CO_2 in Krebs solution prior to FRET readings. All cardiomyocyte FRET experiments were performed using the Opera Phenix™ High Content Screening System (PerkinElmer) with the confocal setting at 40X magnification at 37°C and 5% CO_2 and analyzed with Columbus Image Analysis System (PerkinElmer). Each well was excited with 425 nm light and emissions detected at 434-515 nm for CFP and 500-550 nm for YFP. Basal FRET images were obtained prior to addition of agonist and stimulated FRET images were obtained 15 minutes after addition of agonist to indicated final concentration. For experiments requiring a β-AR antagonist, 1 μM alprenolol was added to cardiomyocytes 30 minutes prior to obtaining basal FRET images. The FRET ratio was calculated as YFP emission/CFP emission. For all

experiments, ΔFRET refers to: (Stimulated Agonist FRET Ratio – Basal Agonist FRET Ratio) – (Stimulated vehicle FRET Ratio – Basal FRET Ratio). The average of three technical replicates was taken for all treatments.

Following FRET experiments, cardiomyocytes were stained with 5 μM Draq5 at room temperature for 5 minutes. Images were obtained on the Opera Phenix™ High Content Screening System (PerkinElmer) using the confocal setting at 40X magnification. Draq5 was imaged using 640 nm excitation and emissions detected at 650-760 nm, YFP using 425 nm excitation and emission detected at 434-515 nm, and CFP using 425 nm excitation and emission detected at 500-550 nm.

RT-qPCR

Following indicated treatments of cardiomyocytes, cells were lysed in TRI reagent and RNA was extracted following the manufacturer's protocol. Reverse transcription was performed with random hexamer primers using an MMLV-RT platform (Promega) according to the manufacturer's protocol. Subsequent qPCR analysis was performed with BrightGreen 2x qPCR Master mix (Applied Biological Materials Inc.) on a Bio-Rad 1000 Series Thermal Cycling CFX96 Optical Reaction module. Ct values were normalized to U6 snRNA and fold change over respective control was calculated using $2^{-\Delta\Delta Ct}$ method. Primer sequences were the following: Nppb (5' CAATCCACGATGCAGAAGCTG 3' and 5' TTTTGTAGGGCCTTGGTCCTTT 3'), Nppa (5' CCTGGACTGGGGAAGTCAAC 3' and 5' ATCTATCGGAGGGGTCCCAG 3'), Serpine1 (5' TCCTCGGTGCTGGCTATGCT 3' and 5' TGGAGAGCTTTCGGAGGGCA 3'), and U6 snRNA (5' TGGAACGATACAGAGAAGATTAG 3' and 5' GAATTTGCGTGTCATCCTTG 3').

504

505 **RNA-seq analysis**

506 RNA was isolated with the RNeasy® Mini Kit (Qiagen) according to manufacturer's
507 instructions. Libraries were prepared using the NEBNext® rRNA-depleted (HMR) stranded
508 library kit and single-read 50bp sequencing completed on the Illumina HiSeq 4000 at the McGill
509 University and Génome Québec Innovation Centre, Montréal, Canada. Reads were trimmed with
510 TrimGalore (0.6.0) (82, 83) using the following settings: --phred33 --length 36 -q 5 --stringency
511 1 -e 0.1. Following processing, reads were aligned to the Ensembl rat reference genome
512 (Rattus_norvegicus.Rnor_6.0.94) (84) with STAR (2.7.1a) (85). Transcripts were assembled
513 with StringTie (1.3.4d) (86) and imported into R (3.6.1) with tximport (1.12.3) (87). Differential
514 gene expression was assessed with DESeq2 (1.24.0) (88) with the independent hypothesis
515 weighting (IHW) library for multiple testing adjustment (89). Heatmaps and K-means clustering
516 was completed with pheatmap and the removeBatchEffect function from limma (3.40.6) (90)
517 was used prior to data visualization. Pathway analysis was completed with Ingenuity Pathway
518 Analysis *(IPA, QIAGEN Inc., https://www.qiagenbio- informatics.com/products/ingenuity-*
519 *pathway-analysis*) (91).

520

521 **Chromatin immunoprecipitation-qPCR**

522 Preparation and immunoprecipitation of cardiomyocyte chromatin was performed as
523 previously described, with minor modifications (92). Following the indicated treatments,
524 cardiomyocytes were crosslinked with 1% formaldehyde in DMEM low glucose for 10 min at
525 room temperature with slight agitation. Crosslinking was quenched by addition of glycine to 125
526 mM final concentration and incubated for 5 min at room temperature with slight agitation.

Cardiomyocytes were placed on ice following fixation, washed once with cold PBS, scraped into PBS with 1 mM PMSF and pelleted at 800 g for 5 min at 4°C. The pellet was resuspended in lysis buffer (10 mM Tris-HCl pH 8.0, 10 mM EDTA, 0.5 mM EGTA, 0.25% Triton X-100, 1 mM PMSF, 1x protease inhibitor cocktail) and incubated for 10 min at 4°C on a nutator. Nuclei were pelleted at 800 g for 5 min at 4°C and resuspended in nuclei lysis buffer (50 mM TrisHCl pH 8.0, 10 mM EDTA, 1% SDS, 1 mM PMSF, 1x protease inhibitor cocktail). Nuclei were incubated for 15 min on ice followed by sonication with a BioRuptor (Diagenode) (18 cycles, 30 s on/off, high power). Insoluble cellular debris was removed by centrifugation at 14 000 g for 10 min at 4°C. A small aliquot was taken for quantification and the remaining sample stored at -80°C until use. The aliquot was incubated at 65°C overnight to reverse crosslinks, treated with RNase A (50 µg/mL) for 15 min at 37°C, and then treated with proteinase K (200 µg/mL) for 1.5 h at 42°C. Protein was removed by phenol/chloroform extraction and DNA precipitated at -80°C with 0.3M sodium acetate pH 5.2, 2.5 volumes of 100% ethanol, and 20 µg of glycogen. Samples were centrifuged for 20 min at 16 000 g, the pellet was washed with 70% ethanol, resuspended with ddH_2O and quantified using a NanoDrop spectrophotometer (Thermo Fisher) to determine concentration of chromatin for each sample.

For immunoprecipitations, 10 µg of chromatin was diluted 9x with dilution buffer (16.7 mM Tris-HCl pH 8.0, 1.2 mM EDTA, 167 mM NaCl, 0.01% SDS, 1.1% Triton X-100, 1x protease inhibitor cocktail). *S. pombe* chromatin, prepared as previously described (93), was spiked-in to each sample for normalization. A rabbit anti-Brd4 antibody (Bethyl, A301-985A; 5ug) or rabbit IgG antibody (Millipore, 12-370; 5 µg), as well as anti-*S. pombe* H2B antibody (Abcam, ab188271), were added to respective IPs and 1% input sample taken for subsequent analysis. Each IP was incubated at 4°C overnight on a nutator, followed by addition of 15 µL

Protein G Dynabeads (Invitrogen) in dilution buffer for 4 h. Beads were washed 2X with low salt buffer (20 mM Tris-HCl pH 8.0, 2 mM EDTA, 150 mM NaCl, 0.1% SDS, 1% Triton X-100), 2X with high salt buffer (20 mM Tris-HCl pH 8.0, 2 mM EDTA, 500 mM NaCl, 0.1% SDS, 1% Triton X-100), 1X with LiCl buffer (10 mM Tris pH 8.0, 1 mM EDTA, 0.25M LiCl, 1% NP-40, 1% deoxycholate), 1X with TE buffer (10mM Tris-HCl pH 8.0, 1 mM EDTA) at 4°C. Beads were resuspended in elution buffer (200 mM NaCl, 1% (w/v) SDS) and heated at 65°C for 20 min to elute chromatin. The eluted chromatin was incubated at 65°C overnight to reverse crosslinks and then incubated with proteinase K (200 μg/mL) for 2 h at 37°C. DNA was purified and quantified as described above.

Localization was assessed by qPCR with primers for specific genomic loci; a primer pair amplifying *S. pombe cdc2*$^{+}$ was used for normalization. All qPCR reactions were performed using a Bio-Rad 1000 Series Thermal Cycling CFX96 Optical Reaction module and iQ SYBR Green Supermix (Bio-Rad). For each primer pair in a given experimental condition, percent input for IgG control IP was subtracted from the percent input for the Brd4 IP, followed by normalization to the percent input of *S. pombe cdc2*$^{+}$. Primer sequences were the following: Nppb SE (chr5:164778453-164778528, 5' AGGTGGCACCCCCTCTTCTAC 3' and 5' TTGGGGGAGTCTCAGCAGCTT 3'), Nppb TSS (chr5:164796330-164796402, 5' TTTCCTTAATCTGTCGCCGC 3' and 5' GGATTGTTCTGGAGACTGGC 3'), Nppa TSS (chr5:164808403-164808456, 5' GTGACGGACAAAGGCTGAGA 3' and 5' ATGTTTGCTGTCTCGGCTCA 3'), Serpine1 SE #1 (chr12:22636488-22636538, 5' TCCCCCGCTAACTCGAACGC 3' and 5' TTGTTTGGAGAGCCACCAGGC 3'), Serpine1 SE #2 (chr12:22634466-22634539, 5' TTGAGTGGCAGACAGCCGACA 3' and 5' GGCGGCCTCCAACATTCCTC 3'), Serpine1 TSS (chr12:22640931-22641011, 5'

AGCCCCACCCACCTTCTAACTC 3' and 5' TACTGGGAGGGAGGGAAGGAGA 3'), Ctgf SE #1 (chr1:21871291-21871393, 5' AGCCCTGGAATGCTGTTT 3' and 5' ACCGCATGATATCTCCTAAACC 3'), Ctgf SE #2 (chr1:21984665-21984753, 5' AGTGAGTCAGGGAGGAAGAA 3' and 5' CTCCTGCAGCCTGTGATTAG 3'), Ctgf TSS (chr1:21854660-21854725, 5' CAGACCCACTCCAGCTCCGA 3' and 5' GTGGCTCCTGGGGTTGTCCA 3'), and Fos TSS (chr6:109300463-109300526, 5' GACTGGATAGAGCCGGCGGA 3' and 5' CAGAGCAGAGCTGGGTGGGA 3').

Protein extraction and western blot

Treated cardiomyocytes were lysed in RIPA buffer (1% NP-40, 50 mM Tris-HCl pH 7.4, 150 mM NaCl, 1 mM EDTA, 1 mM EGTA, 0.1% SDS, 0.5% sodium deoxycholate) and protein quantified by Bradford assay. Proteins were denatured at 65°C for 15 min in Laemmilli buffer and protein expression was assessed by western blot. Western blots were probed with anti-Brd4 (Bethyl, A301-985A; 1:1000) or anti-Hsp90 (Enzo Life Sciences, AC88; 1:1000) in 5% milk overnight at 4°C. The following day, blots were visualized with peroxidase-conjugated secondary antibodies and an Amersham™ Imager 600.

Statistical Analysis

All statistical analysis was performed using GraphPad Prism 8 software. Two-way analysis of variance was performed followed by post-hoc t-tests with Bonferroni correction (Figure 1B, Figure 2B/C/E, Figure 3B/C, Figure 5B/C, Figure 9A/C). Unpaired t-test was completed for validation of gene knockdown by siRNA (Figure 2D, Figure 5A) and for Brd4 ChIP with forskolin and IBMX (Figure 9B). One-way analysis of variance followed by

Dunnett's post-hoc comparison was performed for Brd4 ChIP (Figure 6A) and Brd4 protein expression (Figure 6C) following 24 h receptor activation. For the upstream regulator prediction (Figure 7G), the p-value was obtained by a Fisher's Exact Test completed within the Ingenuity Pathway Analysis software.

Figure Legends

Figure 1. Inhibition of the P-TEFb kinase subunit Cdk9 prevents cardiomyocyte hypertrophy in response to α1-AR or ETR activation. **(A)** NRCMs were treated with PE or ET-1 for 24 h as indicated. Cardiomyocytes were stained with Hoechst dye and identified by staining for the cardiomyocyte-specific marker α_2-actinin. **(B)** Fold change in cardiomyocyte surface area following 24 h treatment over the surface area of cardiomyocytes from the same biological replicate at 0 h. Data is presented as mean ± S.E.M with each point representing a biological replicate. Two-way ANOVA followed by post-hoc t-tests with Bonferroni correction was performed (***p<0.001, ****p<0.0001).

Figure 2. **Disruption of SEC-P-TEFb interaction blocks the hypertrophic response following activation of either receptor. (A)** NRCMs were treated for 24 h as indicated. Cardiomyocytes were stained with Hoechst dye and identified by staining of the cardiomyocyte-specific marker α_2-actinin. **(B)** Fold change in surface area of identified cardiomyocytes over siRNA control-transfected cardiomyocytes from the same biological replicate at 0 h. Two-way ANOVA followed by post-hoc t-tests with Bonferroni correction was performed. **(C)** Expression of three genes previously identified as upregulated in hypertrophic cardiomyocytes, Nppb, Nppa and Serpine1, was determined by RT-qPCR. Two-way ANOVA followed by post-hoc t-tests

with Bonferroni correction was performed. **(D)** Aff4 knockdown in cardiomyocytes 72 h after transfection with Aff4 targeted siRNA was validated by RT-qPCR. An unpaired t-test was performed. **(E)** Fold change in surface area of identified cardiomyocytes over the surface area of siRNA control-transfected cardiomyocytes from the same biological replicate at 0 h. Cardiomyocytes were transfected 72 h prior to treatment with 50 nM of the specified siRNA. Data is presented as mean ± S.E.M with each point representing a biological replicate. Two-way ANOVA followed by post-hoc t-tests with Bonferroni correction was performed (*p<0.05, **p<0.01, ***p<0.001, ****p<0.0001).

Figure 3. **Effects of BET inhibitor JQ1 on cardiomyocyte hypertrophy are specific to the receptor driving the response. (A)** NRCMs treated for 24 h were fixed and stained with Hoechst dye and identified by staining for the cardiomyocyte-specific marker α_2-actinin. **(B)** Fold change in surface area of cardiomyocytes over surface area of cardiomyocytes at 0 h from the same biological replicate. Two-way ANOVA followed by post-hoc t-tests with Bonferroni correction was performed. **(C)** Expression of genes previously demonstrated to be upregulated in hypertrophic cardiomyocytes was determined by RT-qPCR. Data is presented as mean ± S.E.M with each point representing a biological replicate. Two-way ANOVA followed by post-hoc t-tests with Bonferroni correction was performed (**p<0.01, ***p<0.001, ****p<0.0001).

Figure 4. ETR-mediated hypertrophy is insensitive to BET inhibition independent of ET-1 concentration. Dose response curves were generated to assess the effect of JQ1 on cardiomyocyte surface area at a range of ET-1. Cardiomyocytes were treated for 24 h as indicated followed by fixation and staining with Hoechst dye and for α_2-actinin to identify

642 NCRMs. Fold change in surface area over cardiomyocytes from the same biological replicate at
643 0 h was determined. Data is presented as mean ± S.E.M for n=3-4 independent experiments.
644 Dose response curves were plotted using sigmoidal dose response (variable slope) curves by
645 non-linear regression.
646
647 **Figure 5. Role of individual BET family members expressed in cardiomyocytes assessed**
648 **after siRNA-mediated knockdown. (A)** Brd2, Brd3, and Brd4 knockdown efficiency in
649 NRCMs 72 h after transfection with targeted siRNA was determined by RT-qPCR. An unpaired
650 t-test was performed. **(B)** Fold change in surface area over cardiomyocytes transfected with
651 control siRNA from the same biological replicate at 0 h. Following 72 h knockdown with
652 indicated siRNA, cardiomyocytes were treated for 24 h as indicted. Cardiomyocytes were fixed
653 and identified by staining for the cardiomyocyte specific marker α_2-actinin. Two-way ANOVA
654 followed by post-hoc t-tests with Bonferroni correction was performed. **(C)** Change in
655 cardiomyocyte size from (B) is presented relative to respective vehicle/siRNA treatment to
656 normalize for the difference in basal size. Data is presented as mean ± S.E.M with each point
657 representing a biological replicate. Two-way ANOVA followed by post-hoc t-tests with
658 Bonferroni correction was performed (*$p<0.05$, **$p<0.01$, ***$p<0.001$).
659
660 **Figure 6. Brd4 chromatin occupancy increases in response to α_1-AR but not ETR**
661 **activation. (A)** Cardiomyocytes were treated for 24 h as indicated. Following treatment,
662 crosslinked chromatin was immunoprecipitated with an anti-Brd4 antibody, followed by DNA
663 purification and quantification by qPCR using primers at the indicated loci. Each
664 immunoprecipitation was normalized to the % input for exogenous *S. pombe* spike-in DNA at

665 the *cdc2*$^{+}$ loci. Data was analyzed by one-way ANOVA followed by Dunnett's post-hoc
666 comparison. **(B)** A western blot to assess changes in Brd4 protein expression following the
667 indicated treatment for 24 h. **(C)** Densitometry based quantification of Brd4 normalized to Hsp90
668 expression. Data is presented as mean ± S.E.M with each point representing a biological
669 replicate. Data was analyzed by one-way ANOVA followed by Dunnett's post-hoc comparison
670 (*p<0.05, **p<0.01).
671
672 **Figure 7. Transcriptome analysis of gene expression programs mediated by receptor**
673 **activation and the effect of Brd4 inhibition. (A)** Venn diagram of significantly upregulated
674 genes (log2FC > 1 for Agonist/Vehicle vs Vehicle/Vehicle, p-value < 0.05) or **(B)**
675 downregulated genes (log2FC < -1 for Agonist/Vehicle vs Vehicle/Vehicle, p-value < 0.05)
676 following 24 h receptor activation. **(C and D)** Heat maps were generated for genes differentially
677 regulated following activation of the specified receptor for 24 h. Each row was normalized, with
678 the color representing the z-score for the specific row. K-means clustering was performed to
679 identify subsets of genes with distinct patterns following Brd4 inhibition. **(E)** Venn diagram of
680 genes upregulated by respective receptor activation (log2FC > 1 for Agonist/Vehicle vs
681 Vehicle/Vehicle, p-value < 0.05) and attenuated by Brd4 inhibition from the activated state
682 (log2FC < -0.5 for Agonist/JQ1 vs Agonist/Vehicle, p-value < 0.05). **(F)** Gene ontology
683 enrichment for genes attenuated by JQ1 following receptor activation (from E) performed with
684 DAVID. The false discovery rate (FDR) indicates whether the pathway was significantly
685 enriched in the gene list. **(G)** Changes in transcription factor activity predicted by Ingenuity
686 Pathway Analysis (IPA). The z-score represents the predicted change in transcription factor
687 activity between the two treatment groups and the p-value indicates whether the transcription

688 factor's targets are significantly enriched in the gene set. The purple dots (left side) indicate the
689 change in activity following agonist treatment alone (log2FC > 1 for Agonist/Vehicle vs
690 Vehicle/Vehicle, p-value < 0.05). The green dots (right side) indicate the JQ1 dependent
691 decrease in activity from the activated state (log2FC < -0.5 for Agonist/JQ1 vs Agonist/Vehicle,
692 p-value < 0.05).
693
694 **Figure 8. α_1-AR activation leads to increased nuclear PKA signalling. (A)** Cardiomyocytes
695 were transduced with AAV9-AKAR4-NLS virus at a MOI of 5000 and imaged 72 h later. Nuclei
696 were visualized by staining live cells with Draq5. **(B)** Dose-response curves for PKA activation
697 following activation of the ETR or α_1-AR were generated. Alprenolol was included to prevent
698 off-target β-AR activation by high concentrations of PE. Data is presented mean ± S.E.M for
699 three biological replicates. Dose response curves were plotted using sigmoidal dose response
700 (variable slope) curves by non-linear regression.
701
702 **Figure 9. PKA signalling regulates recruitment of Brd4 to chromatin. (A and B)** Effect of
703 PKA inhibition with the small-molecule inhibitor KT5720 on receptor-mediated increases in
704 Brd4 occupancy. Cardiomyocytes were pre-treated for 30 min with the PKA inhibitor prior to
705 receptor activation for 1.5 h with the indicated agonists. Two-way ANOVA followed by post-
706 hoc t-test comparisons with Bonferroni correction was performed. **(C)** PKA was activated for 1.5
707 h by increasing intracellular cAMP levels with forskolin and IBMX, an adenylyl cyclase
708 activator and phosphodiesterase inhibitor respectively. Following indicated treatment,
709 cardiomyocytes were fixed, and ChIP was performed with an anti-Brd4 antibody. ChIP was
710 quantified by qPCR using primers at the indicated loci. An unpaired t-test was performed. **(D)**

After 24 h of the indicated treatments, NRCMs were fixed and stained with Hoechst dye and for the cardiomyocyte specific marker α_2-actinin. **(E)** Fold change in surface area after 24 h of the indicated treatment over cardiomyocytes fixed at 0 h from the same biological replicate. Two-way ANOVA followed by post-hoc t-test comparisons with Bonferroni correction was performed. Data is presented as mean ± S.E.M with each point representing a separate biological replicate. (*p<0.05, ***p<0.001, ****p<0.0001).

Figure 10. **Model of P-TEFb complex activation following activation of the α_1-AR or ETR.** Both the ETR and α_1-AR activate a signalling cascade which increases active P-TEFb and requires subsequent recruitment through the SEC. The α_1-AR activation also leads to Brd4-dependent recruitment due to the activation of a PKA signalling pathway.

Acknowledgements

This work was supported by a grant from the Heart and Stroke Foundation of Canada (G-15-0008938) to T.E.H and J.C.T, a grant from Canadian Institute of Health Science (CIHR) (MOP 130-362) to J.C.T. and a grant from CIHR (PJT 159687) to T.E.H. R.M. was supported by a studentship from the McGill-CIHR Drug Development Training Program and McGill Faculty of Medicine. We thank Dr. Jin Zhang (UCSD), Dr. Karel Svoboda, and Novartis Institutes for Biomedical Research (Emeryville, CA) for providing materials instrumental to this study. We thank the McGill Imaging and Molecular Biology Platform for assistance with our high-content

733 microscopy experiments. Lastly, we thank all the members of Dr. Hébert and Dr. Tanny's labs
734 for discussions and critical reading of the manuscript.

735

736 **References**

737 1. Sutton MG, Sharpe N. 2000. Left ventricular remodeling after myocardial infarction:
738 pathophysiology and therapy. Circulation 101:2981-8.
739 2. Nadruz W. 2015. Myocardial remodeling in hypertension. J Hum Hypertens 29:1-6.
740 3. Gerdes AM. 2002. Cardiac myocyte remodeling in hypertrophy and progression to
741 failure. J Card Fail 8:S264-8.
742 4. Hill JA, Olson EN. 2008. Cardiac plasticity. N Engl J Med 358:1370-80.
743 5. Heineke J, Molkentin JD. 2006. Regulation of cardiac hypertrophy by intracellular
744 signalling pathways. Nat Rev Mol Cell Biol 7:589-600.
745 6. van Berlo JH, Maillet M, Molkentin JD. 2013. Signaling effectors underlying pathologic
746 growth and remodeling of the heart. J Clin Invest 123:37-45.
747 7. D'Angelo DD, Sakata Y, Lorenz JN, Boivin GP, Walsh RA, Liggett SB, Dorn GW, 2nd.
748 1997. Transgenic Gαq overexpression induces cardiac contractile failure in mice. Proc
749 Natl Acad Sci U S A 94:8121-6.
750 8. Iwase M, Bishop SP, Uechi M, Vatner DE, Shannon RP, Kudej RK, Wight DC, Wagner
751 TE, Ishikawa Y, Homcy CJ, Vatner SF. 1996. Adverse effects of chronic endogenous
752 sympathetic drive induced by cardiac GS alpha overexpression. Circ Res 78:517-24.
753 9. Akazawa H, Komuro I. 2003. Roles of cardiac transcription factors in cardiac
754 hypertrophy. Circ Res 92:1079-88.

10. Ho MK, Su Y, Yeung WW, Wong YH. 2009. Regulation of transcription factors by heterotrimeric G proteins. Curr Mol Pharmacol 2:19-31.

11. Sano M, Abdellatif M, Oh H, Xie M, Bagella L, Giordano A, Michael LH, DeMayo FJ, Schneider MD. 2002. Activation and function of cyclin T-Cdk9 (positive transcription elongation factor-b) in cardiac muscle-cell hypertrophy. Nat Med 8:1310-7.

12. Papait R, Cattaneo P, Kunderfranco P, Greco C, Carullo P, Guffanti A, Vigano V, Stirparo GG, Latronico MV, Hasenfuss G, Chen J, Condorelli G. 2013. Genome-wide analysis of histone marks identifying an epigenetic signature of promoters and enhancers underlying cardiac hypertrophy. Proc Natl Acad Sci U S A 110:20164-9.

13. Zhou Q, Li T, Price DH. 2012. RNA polymerase II elongation control. Annu Rev Biochem 81:119-43.

14. Lin C, Smith ER, Takahashi H, Lai KC, Martin-Brown S, Florens L, Washburn MP, Conaway JW, Conaway RC, Shilatifard A. 2010. AFF4, a component of the ELL/P-TEFb elongation complex and a shared subunit of MLL chimeras, can link transcription elongation to leukemia. Mol Cell 37:429-37.

15. Jang MK, Mochizuki K, Zhou M, Jeong HS, Brady JN, Ozato K. 2005. The bromodomain protein Brd4 is a positive regulatory component of P-TEFb and stimulates RNA polymerase II-dependent transcription. Mol Cell 19:523-34.

16. Shi J, Vakoc CR. 2014. The mechanisms behind the therapeutic activity of BET bromodomain inhibition. Mol Cell 54:728-36.

17. Bisgrove DA, Mahmoudi T, Henklein P, Verdin E. 2007. Conserved P-TEFb-interacting domain of BRD4 inhibits HIV transcription. Proc Natl Acad Sci U S A 104:13690-5.

18. Anand P, Brown JD, Lin CY, Qi J, Zhang R, Artero PC, Alaiti MA, Bullard J, Alazem K, Margulies KB, Cappola TP, Lemieux M, Plutzky J, Bradner JE, Haldar SM. 2013. BET bromodomains mediate transcriptional pause release in heart failure. Cell 154:569-82.

19. Stratton MS, Lin CY, Anand P, Tatman PD, Ferguson BS, Wickers ST, Ambardekar AV, Sucharov CC, Bradner JE, Haldar SM, McKinsey TA. 2016. Signal-Dependent Recruitment of BRD4 to Cardiomyocyte Super-Enhancers Is Suppressed by a MicroRNA. Cell Rep 16:1366-1378.

20. Duan Q, McMahon S, Anand P, Shah H, Thomas S, Salunga HT, Huang Y, Zhang R, Sahadevan A, Lemieux ME, Brown JD, Srivastava D, Bradner JE, McKinsey TA, Haldar SM. 2017. BET bromodomain inhibition suppresses innate inflammatory and profibrotic transcriptional networks in heart failure. Sci Transl Med 9.

21. Spiltoir JI, Stratton MS, Cavasin MA, Demos-Davies K, Reid BG, Qi J, Bradner JE, McKinsey TA. 2013. BET acetyl-lysine binding proteins control pathological cardiac hypertrophy. J Mol Cell Cardiol 63:175-9.

22. Luo Z, Lin C, Shilatifard A. 2012. The super elongation complex (SEC) family in transcriptional control. Nat Rev Mol Cell Biol 13:543-7.

23. Lin C, Garrett AS, De Kumar B, Smith ER, Gogol M, Seidel C, Krumlauf R, Shilatifard A. 2011. Dynamic transcriptional events in embryonic stem cells mediated by the super elongation complex (SEC). Genes Dev 25:1486-98.

24. Biswas D, Milne TA, Basrur V, Kim J, Elenitoba-Johnson KS, Allis CD, Roeder RG. 2011. Function of leukemogenic mixed lineage leukemia 1 (MLL) fusion proteins through distinct partner protein complexes. Proc Natl Acad Sci U S A 108:15751-6.

799 25. Izumi K, Nakato R, Zhang Z, Edmondson AC, Noon S, Dulik MC, Rajagopalan R,
800 Venditti CP, Gripp K, Samanich J, Zackai EH, Deardorff MA, Clark D, Allen JL, Dorsett
801 D, Misulovin Z, Komata M, Bando M, Kaur M, Katou Y, Shirahige K, Krantz ID. 2015.
802 Germline gain-of-function mutations in AFF4 cause a developmental syndrome
803 functionally linking the super elongation complex and cohesin. Nat Genet 47:338-44.
804 26. Wang J, Gareri C, Rockman HA. 2018. G-Protein-Coupled Receptors in Heart Disease.
805 Circ Res 123:716-735.
806 27. Clerk A, Sugden PH. 1997. Regulation of phospholipases C and D in rat ventricular
807 myocytes: stimulation by endothelin-1, bradykinin and phenylephrine. J Mol Cell Cardiol
808 29:1593-604.
809 28. Galvez AS, Brunskill EW, Marreez Y, Benner BJ, Regula KM, Kirschenbaum LA, Dorn
810 GW, 2nd. 2006. Distinct pathways regulate proapoptotic Nix and BNip3 in cardiac stress.
811 J Biol Chem 281:1442-8.
812 29. Hong HM, Song EJ, Oh E, Kabir MH, Lee C, Yoo YS. 2011. Endothelin-1- and
813 isoproterenol-induced differential protein expression and signaling pathway in HL-1
814 cardiomyocytes. Proteomics 11:283-97.
815 30. Lu H, Xue Y, Yu GK, Arias C, Lin J, Fong S, Faure M, Weisburd B, Ji X, Mercier A,
816 Sutton J, Luo K, Gao Z, Zhou Q. 2015. Compensatory induction of MYC expression by
817 sustained CDK9 inhibition via a BRD4-dependent mechanism. Elife 4:e06535.
818 31. Li Y, Liu M, Chen LF, Chen R. 2018. P-TEFb: Finding its ways to release promoter-
819 proximally paused RNA polymerase II. Transcription 9:88-94.
820 32. Liang K, Smith ER, Aoi Y, Stoltz KL, Katagi H, Woodfin AR, Rendleman EJ, Marshall
821 SA, Murray DC, Wang L, Ozark PA, Mishra RK, Hashizume R, Schiltz GE, Shilatifard

A. 2018. Targeting Processive Transcription Elongation via SEC Disruption for MYC-Induced Cancer Therapy. Cell 175:766-779 e17.

33. Filippakopoulos P, Qi J, Picaud S, Shen Y, Smith WB, Fedorov O, Morse EM, Keates T, Hickman TT, Felletar I, Philpott M, Munro S, McKeown MR, Wang Y, Christie AL, West N, Cameron MJ, Schwartz B, Heightman TD, La Thangue N, French CA, Wiest O, Kung AL, Knapp S, Bradner JE. 2010. Selective inhibition of BET bromodomains. Nature 468:1067-73.

34. Gordon JW, Shaw JA, Kirshenbaum LA. 2011. Multiple facets of NF-κB in the heart: to be or not to NF-κB. Circ Res 108:1122-32.

35. Wu SY, Lee AY, Lai HT, Zhang H, Chiang CM. 2013. Phospho switch triggers Brd4 chromatin binding and activator recruitment for gene-specific targeting. Mol Cell 49:843-57.

36. Martin RD, Sun Y, Bourque K, Audet N, Inoue A, Tanny JC, Hébert TE. 2018. Receptor- and cellular compartment-specific activation of the cAMP/PKA pathway by α_1-adrenergic and ETA endothelin receptors. Cell Signal 44:43-50.

37. Depry C, Allen MD, Zhang J. 2011. Visualization of PKA activity in plasma membrane microdomains. Mol Biosyst 7:52-8.

38. Kase H, Iwahashi K, Nakanishi S, Matsuda Y, Yamada K, Takahashi M, Murakata C, Sato A, Kaneko M. 1987. K-252 compounds, novel and potent inhibitors of protein kinase C and cyclic nucleotide-dependent protein kinases. Biochem Biophys Res Commun 142:436-40.

39. Boularan C, Gales C. 2015. Cardiac cAMP: production, hydrolysis, modulation and detection. Front Pharmacol 6:203.

40. Morisco C, Zebrowski DC, Vatner DE, Vatner SF, Sadoshima J. 2001. β-adrenergic cardiac hypertrophy is mediated primarily by the β(1)-subtype in the rat heart. J Mol Cell Cardiol 33:561-73.

41. de Lucia C, Eguchi A, Koch WJ. 2018. New Insights in Cardiac β-Adrenergic Signaling During Heart Failure and Aging. Front Pharmacol 9:904.

42. Tan Y, Wang L, Du Y, Liu X, Chen Z, Weng X, Guo J, Chen H, Wang M, Wang X. 2018. Inhibition of BRD4 suppresses tumor growth in prostate cancer via the enhancement of FOXO1 expression. Int J Oncol 53:2503-2517.

43. Lu L, Chen Z, Lin X, Tian L, Su Q, An P, Li W, Wu Y, Du J, Shan H, Chiang CM, Wang H. 2020. Inhibition of BRD4 suppresses the malignancy of breast cancer cells via regulation of Snail. Cell Death Differ 27:255-268.

44. Dai X, Gan W, Li X, Wang S, Zhang W, Huang L, Liu S, Zhong Q, Guo J, Zhang J, Chen T, Shimizu K, Beca F, Blattner M, Vasudevan D, Buckley DL, Qi J, Buser L, Liu P, Inuzuka H, Beck AH, Wang L, Wild PJ, Garraway LA, Rubin MA, Barbieri CE, Wong KK, Muthuswamy SK, Huang J, Chen Y, Bradner JE, Wei W. 2017. Prostate cancer-associated SPOP mutations confer resistance to BET inhibitors through stabilization of BRD4. Nat Med 23:1063-1071.

45. Stratton MS, McKinsey TA. 2015. Acetyl-lysine erasers and readers in the control of pulmonary hypertension and right ventricular hypertrophy. Biochem Cell Biol 93:149-57.

46. Wang R, Cao XJ, Kulej K, Liu W, Ma T, MacDonald M, Chiang CM, Garcia BA, You J. 2017. Uncovering BRD4 hyperphosphorylation associated with cellular transformation in NUT midline carcinoma. Proc Natl Acad Sci U S A 114:E5352-E5361.

867 47. Shu S, Lin CY, He HH, Witwicki RM, Tabassum DP, Roberts JM, Janiszewska M, Huh
868 SJ, Liang Y, Ryan J, Doherty E, Mohammed H, Guo H, Stover DG, Ekram MB, Brown
869 J, D'Santos C, Krop IE, Dillon D, McKeown M, Ott C, Qi J, Ni M, Rao PK, Duarte M,
870 Wu SY, Chiang CM, Anders L, Young RA, Winer E, Letai A, Barry WT, Carroll JS,
871 Long H, Brown M, Liu XS, Meyer CA, Bradner JE, Polyak K. 2016. Response and
872 resistance to BET bromodomain inhibitors in triple-negative breast cancer. Nature
873 529:413-417.
874 48. Stratton MS, Bagchi RA, Felisbino MB, Hirsch RA, Smith HE, Riching AS, Enyart BY,
875 Koch KA, Cavasin MA, Alexanian M, Song K, Qi J, Lemieux ME, Srivastava D, Lam
876 MPY, Haldar SM, Lin CY, McKinsey TA. 2019. Dynamic Chromatin Targeting of
877 BRD4 Stimulates Cardiac Fibroblast Activation. Circ Res 125:662-677.
878 49. Ha CH, Kim JY, Zhao J, Wang W, Jhun BS, Wong C, Jin ZG. 2010. PKA phosphorylates
879 histone deacetylase 5 and prevents its nuclear export, leading to the inhibition of gene
880 transcription and cardiomyocyte hypertrophy. Proc Natl Acad Sci U S A 107:15467-72.
881 50. Lehmann LH, Worst BC, Stanmore DA, Backs J. 2014. Histone deacetylase signaling in
882 cardioprotection. Cell Mol Life Sci 71:1673-90.
883 51. Kuusisto J, Karja V, Sipola P, Kholova I, Peuhkurinen K, Jaaskelainen P, Naukkarinen
884 A, Yla-Herttuala S, Punnonen K, Laakso M. 2012. Low-grade inflammation and the
885 phenotypic expression of myocardial fibrosis in hypertrophic cardiomyopathy. Heart
886 98:1007-13.
887 52. Erten Y, Tulmac M, Derici U, Pasaoglu H, Altok Reis K, Bali M, Arinsoy T, Cengel A,
888 Sindel S. 2005. An association between inflammatory state and left ventricular
889 hypertrophy in hemodialysis patients. Ren Fail 27:581-9.

890 53. Huang S, Frangogiannis NG. 2018. Anti-inflammatory therapies in myocardial infarction:
891 failures, hopes and challenges. Br J Pharmacol 175:1377-1400.
892 54. Samak M, Fatullayev J, Sabashnikov A, Zeriouh M, Schmack B, Farag M, Popov AF,
893 Dohmen PM, Choi YH, Wahlers T, Weymann A. 2016. Cardiac Hypertrophy: An
894 Introduction to Molecular and Cellular Basis. Med Sci Monit Basic Res 22:75-9.
895 55. Rogatsky I, Adelman K. 2014. Preparing the first responders: building the inflammatory
896 transcriptome from the ground up. Mol Cell 54:245-54.
897 56. Fiordelisi A, Iaccarino G, Morisco C, Coscioni E, Sorriento D. 2019. NFkappaB is a Key
898 Player in the Crosstalk between Inflammation and Cardiovascular Diseases. Int J Mol Sci
899 20.
900 57. Freund C, Schmidt-Ullrich R, Baurand A, Dunger S, Schneider W, Loser P, El-Jamali A,
901 Dietz R, Scheidereit C, Bergmann MW. 2005. Requirement of nuclear factor-κB in
902 angiotensin II- and isoproterenol-induced cardiac hypertrophy in vivo. Circulation
903 111:2319-25.
904 58. Purcell NH, Tang G, Yu C, Mercurio F, DiDonato JA, Lin A. 2001. Activation of NF-κB
905 is required for hypertrophic growth of primary rat neonatal ventricular cardiomyocytes.
906 Proc Natl Acad Sci U S A 98:6668-73.
907 59. Oka T, Maillet M, Watt AJ, Schwartz RJ, Aronow BJ, Duncan SA, Molkentin JD. 2006.
908 Cardiac-specific deletion of Gata4 reveals its requirement for hypertrophy, compensation,
909 and myocyte viability. Circ Res 98:837-45.
910 60. Liang Q, De Windt LJ, Witt SA, Kimball TR, Markham BE, Molkentin JD. 2001. The
911 transcription factors GATA4 and GATA6 regulate cardiomyocyte hypertrophy in vitro
912 and in vivo. J Biol Chem 276:30245-53.

913 61. Omura T, Yoshiyama M, Yoshida K, Nakamura Y, Kim S, Iwao H, Takeuchi K,
914 Yoshikawa J. 2002. Dominant negative mutant of c-Jun inhibits cardiomyocyte
915 hypertrophy induced by endothelin 1 and phenylephrine. Hypertension 39:81-6.
916 62. Chen LF, Williams SA, Mu Y, Nakano H, Duerr JM, Buckbinder L, Greene WC. 2005.
917 NF-κB RelA phosphorylation regulates RelA acetylation. Mol Cell Biol 25:7966-75.
918 63. Huang B, Yang XD, Zhou MM, Ozato K, Chen LF. 2009. Brd4 coactivates
919 transcriptional activation of NF-κB via specific binding to acetylated RelA. Mol Cell Biol
920 29:1375-87.
921 64. Garg R, Caino MC, Kazanietz MG. 2013. Regulation of Transcriptional Networks by
922 PKC Isozymes: Identification of c-Rel as a Key Transcription Factor for PKC-Regulated
923 Genes. PLoS One 8:e67319.
924 65. Katanasaka Y, Suzuki H, Sunagawa Y, Hasegawa K, Morimoto T. 2016. Regulation of
925 Cardiac Transcription Factor GATA4 by Post-Translational Modification in
926 Cardiomyocyte Hypertrophy and Heart Failure. Int Heart J 57:672-675.
927 66. Zhang CL, Xie S, Qiao X, An YM, Zhang Y, Li L, Guo XB, Zhang FC, Wu LL. 2017.
928 Plasma endothelin-1-related peptides as the prognostic biomarkers for heart failure: A
929 PRISMA-compliant meta-analysis. Medicine (Baltimore) 96:e9342.
930 67. Wei CM, Lerman A, Rodeheffer RJ, McGregor CG, Brandt RR, Wright S, Heublein DM,
931 Kao PC, Edwards WD, Burnett JC, Jr. 1994. Endothelin in human congestive heart
932 failure. Circulation 89:1580-6.
933 68. Rodeheffer RJ, Lerman A, Heublein DM, Burnett JC, Jr. 1992. Increased plasma
934 concentrations of endothelin in congestive heart failure in humans. Mayo Clin Proc
935 67:719-24.

936 69. Feyder M, Bonito-Oliva A, Fisone G. 2011. L-DOPA-Induced Dyskinesia and Abnormal
937 Signaling in Striatal Medium Spiny Neurons: Focus on Dopamine D1 Receptor-Mediated
938 Transmission. Front Behav Neurosci 5:71.
939 70. Lynch WJ, Kiraly DD, Caldarone BJ, Picciotto MR, Taylor JR. 2007. Effect of cocaine
940 self-administration on striatal PKA-regulated signaling in male and female rats.
941 Psychopharmacology (Berl) 191:263-71.
942 71. D AF, Standaert DG. 2017. Dysregulation of BET proteins in levodopa-induced
943 dyskinesia. Neurobiol Dis 102:125-132.
944 72. Sartor GC, Powell SK, Brothers SP, Wahlestedt C. 2015. Epigenetic Readers of Lysine
945 Acetylation Regulate Cocaine-Induced Plasticity. J Neurosci 35:15062-72.
946 73. Weigand I, Ronchi CL, Rizk-Rabin M, Dalmazi GD, Wild V, Bathon K, Rubin B,
947 Calebiro D, Beuschlein F, Bertherat J, Fassnacht M, Sbiera S. 2017. Differential
948 expression of the protein kinase A subunits in normal adrenal glands and adrenocortical
949 adenomas. Sci Rep 7:49.
950 74. Calebiro D, Hannawacker A, Lyga S, Bathon K, Zabel U, Ronchi C, Beuschlein F,
951 Reincke M, Lorenz K, Allolio B, Kisker C, Fassnacht M, Lohse MJ. 2014. PKA catalytic
952 subunit mutations in adrenocortical Cushing's adenoma impair association with the
953 regulatory subunit. Nat Commun 5:5680.
954 75. Lee TI, Young RA. 2013. Transcriptional regulation and its misregulation in disease. Cell
955 152:1237-51.
956 76. Lu X, Zhu X, Li Y, Liu M, Yu B, Wang Y, Rao M, Yang H, Zhou K, Wang Y, Chen Y,
957 Chen M, Zhuang S, Chen LF, Liu R, Chen R. 2016. Multiple P-TEFbs cooperatively

regulate the release of promoter-proximally paused RNA polymerase II. Nucleic Acids Res 44:6853-67.

77. Dawson MA, Prinjha RK, Dittmann A, Giotopoulos G, Bantscheff M, Chan WI, Robson SC, Chung CW, Hopf C, Savitski MM, Huthmacher C, Gudgin E, Lugo D, Beinke S, Chapman TD, Roberts EJ, Soden PE, Auger KR, Mirguet O, Doehner K, Delwel R, Burnett AK, Jeffrey P, Drewes G, Lee K, Huntly BJ, Kouzarides T. 2011. Inhibition of BET recruitment to chromatin as an effective treatment for MLL-fusion leukaemia. Nature 478:529-33.

78. Calderone A, Thaik CM, Takahashi N, Chang DL, Colucci WS. 1998. Nitric oxide, atrial natriuretic peptide, and cyclic GMP inhibit the growth-promoting effects of norepinephrine in cardiac myocytes and fibroblasts. J Clin Invest 101:812-8.

79. Yang JH, Polanowska-Grabowska RK, Smith JS, Shields CWt, Saucerman JJ. 2014. PKA catalytic subunit compartmentation regulates contractile and hypertrophic responses to β-adrenergic signaling. J Mol Cell Cardiol 66:83-93.

80. Mao T, Kusefoglu D, Hooks BM, Huber D, Petreanu L, Svoboda K. 2011. Long-range neuronal circuits underlying the interaction between sensory and motor cortex. Neuron 72:111-23.

81. Burger C, Nash KR. 2016. Small-Scale Recombinant Adeno-Associated Virus Purification. Methods Mol Biol 1382:95-106.

82. Krueger F. Trim Galore! http://www.bioinformatics.babraham.ac.uk/projects/trim_galore/. Accessed

83. Martin M. 2011. Cutadapt removes adapter sequences from high-throughput sequencing reads. 2011 17:3.

981 84. Zerbino DR, Achuthan P, Akanni W, Amode MR, Barrell D, Bhai J, Billis K, Cummins
982 C, Gall A, Giron CG, Gil L, Gordon L, Haggerty L, Haskell E, Hourlier T, Izuogu OG,
983 Janacek SH, Juettemann T, To JK, Laird MR, Lavidas I, Liu Z, Loveland JE, Maurel T,
984 McLaren W, Moore B, Mudge J, Murphy DN, Newman V, Nuhn M, Ogeh D, Ong CK,
985 Parker A, Patricio M, Riat HS, Schuilenburg H, Sheppard D, Sparrow H, Taylor K,
986 Thormann A, Vullo A, Walts B, Zadissa A, Frankish A, Hunt SE, Kostadima M,
987 Langridge N, Martin FJ, Muffato M, Perry E, et al. 2018. Ensembl 2018. Nucleic Acids
988 Res 46:D754-D761.
989 85. Dobin A, Davis CA, Schlesinger F, Drenkow J, Zaleski C, Jha S, Batut P, Chaisson M,
990 Gingeras TR. 2013. STAR: ultrafast universal RNA-seq aligner. Bioinformatics 29:15-
991 21.
992 86. Pertea M, Pertea GM, Antonescu CM, Chang TC, Mendell JT, Salzberg SL. 2015.
993 StringTie enables improved reconstruction of a transcriptome from RNA-seq reads. Nat
994 Biotechnol 33:290-5.
995 87. Soneson C, Love MI, Robinson MD. 2015. Differential analyses for RNA-seq: transcript-
996 level estimates improve gene-level inferences. F1000Res 4:1521.
997 88. Love MI, Huber W, Anders S. 2014. Moderated estimation of fold change and dispersion
998 for RNA-seq data with DESeq2. Genome Biol 15:550.
999 89. Ignatiadis N, Klaus B, Zaugg JB, Huber W. 2016. Data-driven hypothesis weighting
1000 increases detection power in genome-scale multiple testing. Nat Methods 13:577-80.
1001 90. Ritchie ME, Phipson B, Wu D, Hu Y, Law CW, Shi W, Smyth GK. 2015. limma powers
1002 differential expression analyses for RNA-sequencing and microarray studies. Nucleic
1003 Acids Res 43:e47.

1004 91. Kramer A, Green J, Pollard J, Jr., Tugendreich S. 2014. Causal analysis approaches in
1005 Ingenuity Pathway Analysis. Bioinformatics 30:523-30.
1006 92. Bolli P, Vardabasso C, Bernstein E, Chaudhry HW. 2013. Chromatin
1007 immunoprecipitation of adult murine cardiomyocytes. Curr Protoc Cell Biol Chapter
1008 17:Unit17 14.
1009 93. Mbogning J, Tanny JC. 2017. Chromatin Immunoprecipitation of Histone Modifications
1010 in Fission Yeast. Methods Mol Biol 1528:199-210.
1011
1012

Figure 1

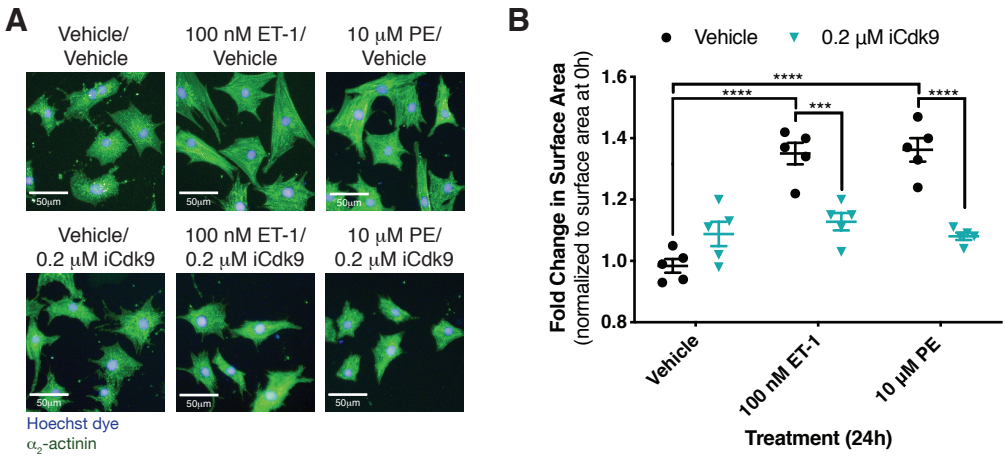

Figure 1. Inhibition of the P-TEFb kinase subunit Cdk9 prevents cardiomyocyte hypertrophy in response to α_1-AR or ETR activation. (A) NRCMs were treated with PE or ET-1 for 24 h as indicated. Cardiomyocytes were stained with Hoechst dye and identified by staining for the cardiomyocyte-specific marker α_2-actinin. (B) Fold change in cardiomyocyte surface area following 24 h treatment over the surface area of cardiomyocytes from the same biological replicate at 0 h. Data is presented as mean ± S.E.M with each point representing a biological replicate. Two-way ANOVA followed by post-hoc t-tests with Bonferroni correction was performed (***p<0.001, ****p<0.0001).

Figure 2

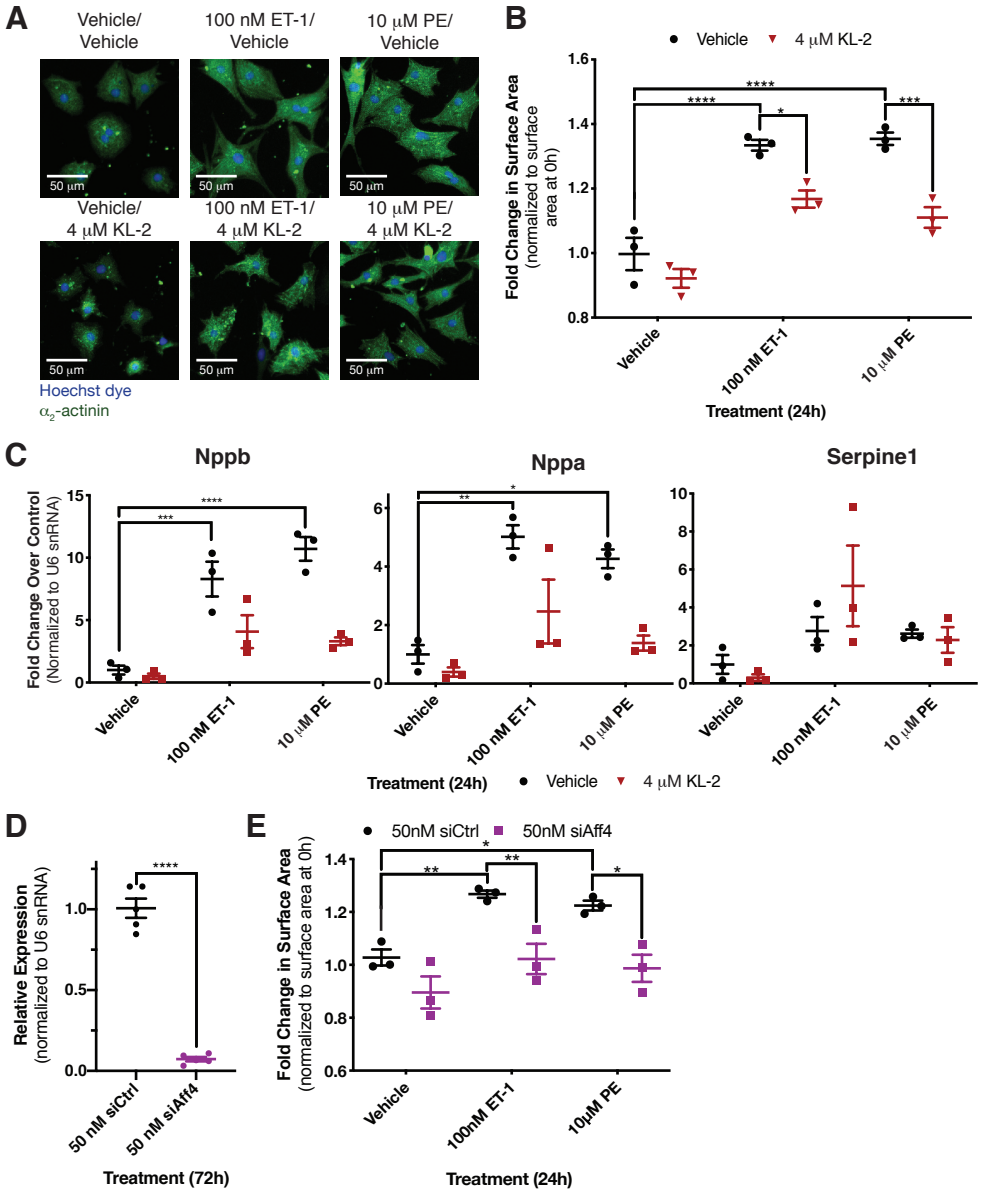

Figure 2. Disruption of SEC-P-TEFb interaction disrupts hypertrophic response following activation of either receptor. (A) NRCMs were treated for 24 h as indicated. Cardiomyocytes were stained with Hoechst dye and identified by staining of the cardiomyocyte-specific marker α_2-actinin. (B) Fold change in surface area of identified cardiomyocytes over siRNA control-transfected cardiomyocytes from the same biological replicate at 0 h. Two-way ANOVA followed by post-hoc t-tests with Bonferroni correction was performed. (C) Expression of three genes previously identified as upregulated in hypertrophic cardiomyocytes, Nppb, Nppa and Serpine1, was determined by RT-qPCR. Two-way ANOVA followed by post-hoc t-tests with Bonferroni correction was performed. (D) Aff4 knockdown in cardiomyocytes 72 h after transfection with Aff4 targeted siRNA was validated by RT-qPCR. An unpaired t-test was performed. (E) Fold change in surface area of identified cardiomyocytes over the surface area of siRNA control-transfected cardiomyocytes from the same biological replicate at 0 h. Cardiomyocytes were transfected 72 h prior to treatment with 50 nM of the specified siRNA. Data is presented as mean ± S.E.M with each point representing a biological replicate. Two-way ANOVA followed by post-hoc t-tests with Bonferroni correction was performed (*p<0.05, **p<0.01, ***p<0.001, ****p<0.0001).

Figure 3

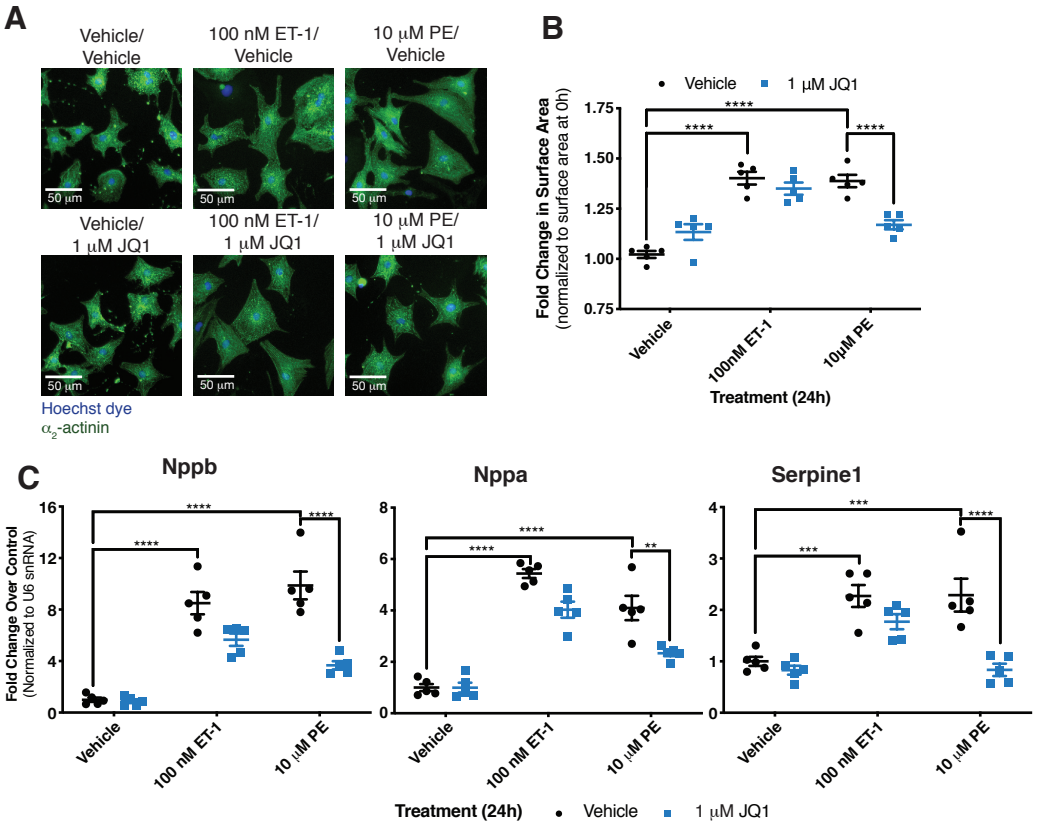

Figure 3. BET family inhibition demonstrates differential mechanisms activated by distinct receptors. (A) NRCMs treated for 24 h were fixed and stained with Hoechst dye and identified by staining for the cardiomyocyte-specific marker α_2-actinin. (B) Fold change in surface area of cardiomyocytes over surface area of cardiomyocytes at 0 h from the same biological replicate. Two-way ANOVA followed by post-hoc t-tests with Bonferroni correction was performed. (C) Expression of genes previously demonstrated to be upregulated in hypertrophic cardiomyocytes was determined by RT-qPCR. Data is presented as mean ± S.E.M with each point representing a biological replicate. Two-way ANOVA followed by post-hoc t-tests with Bonferroni correction was performed (**p<0.01, ***p<0.001, ****p<0.0001).

Figure 4

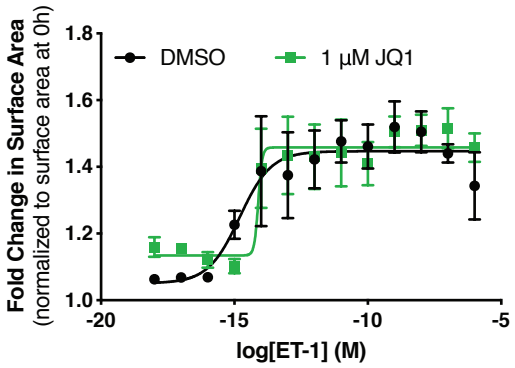

Figure 4. ETR-mediated hypertrophy is insensitive to BET inhibition independent of ET-1 concentration. Dose response curves were generated to assess the effect of JQ1 on cardiomyocyte surface area at a range of ET-1. Cardiomyocytes were treated for 24 h as indicated followed by fixation and staining with Hoechst dye and for α_2-actinin to identify NCRMs. Fold change in surface area over cardiomyocytes from the same biological replicate at 0 h was determined. Data is presented as mean ± S.E.M for n=3-4 independent experiments. Dose response curves were plotted using sigmoidal dose response (variable slope) curves by non-linear regression.

Figure 5

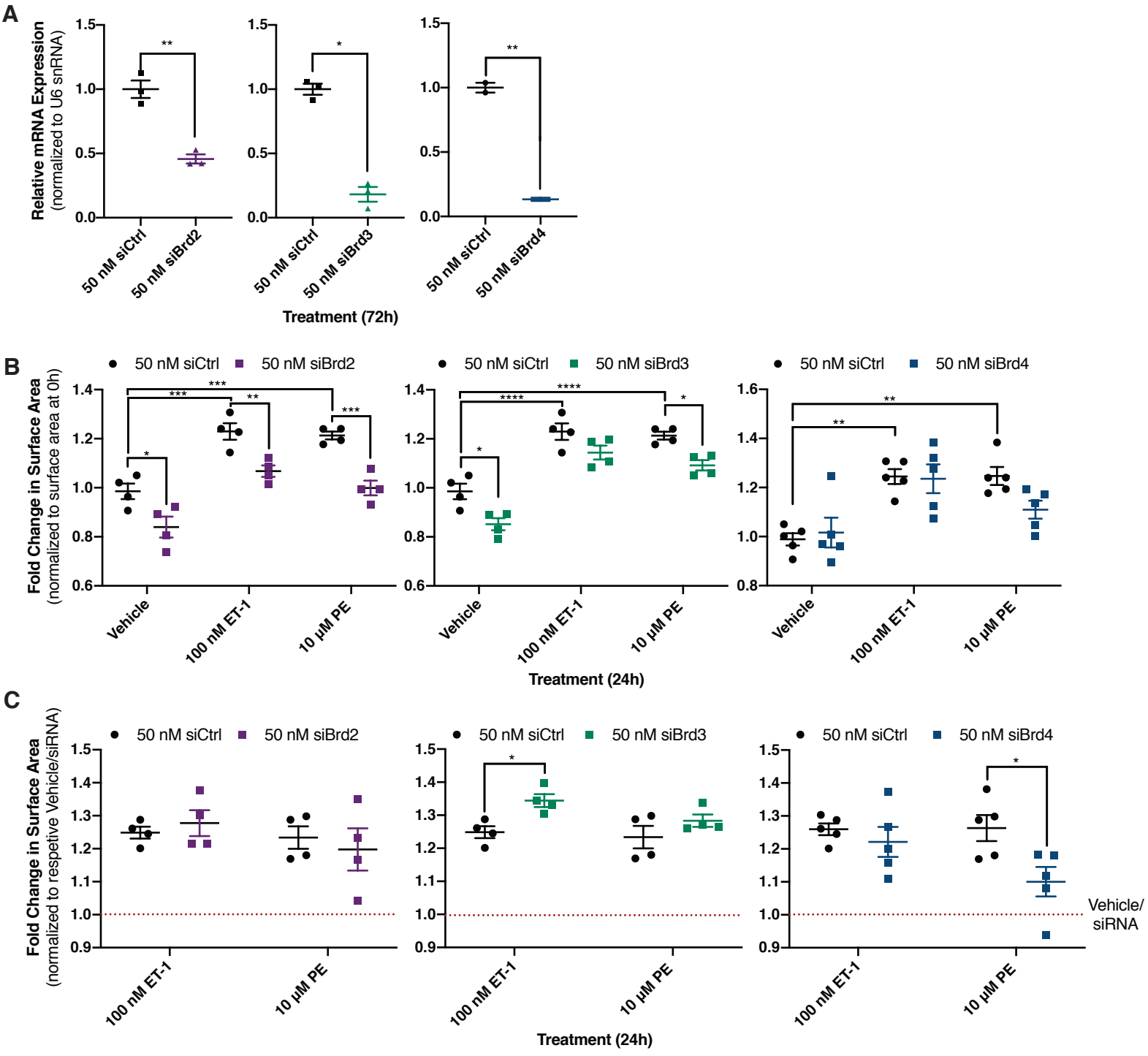

Figure 5. Role of individual BET family members expressed in cardiomyocyte assessed after siRNA-mediated knockdown. (A) Brd2, Brd3, and Brd4 knockdown efficiency in NRCMs 72 h after transfection with targeted siRNA was determined by RT-qPCR. An unpaired t-test was performed. (B) Fold change in surface area over cardiomyocytes transfected with control siRNA from the same biological replicate at 0 h. Following 72 h knockdown with indicated siRNA, cardiomyocytes were treated for 24 h as indicted. Cardiomyocytes were fixed and identified by staining for the cardiomyocyte specific marker α_2-actinin. Two-way ANOVA followed by post-hoc t-tests with Bonferroni correction was performed. (C) Change in cardiomyocyte size from (B) is presented relative to respective vehicle/siRNA treatment to normalize for the difference in basal size. Data is presented as mean ± S.E.M with each point representing a biological replicate. Two-way ANOVA followed by post-hoc t-tests with Bonferroni correction was performed (*p<0.05, **p<0.01, ***p<0.001).

Figure 6

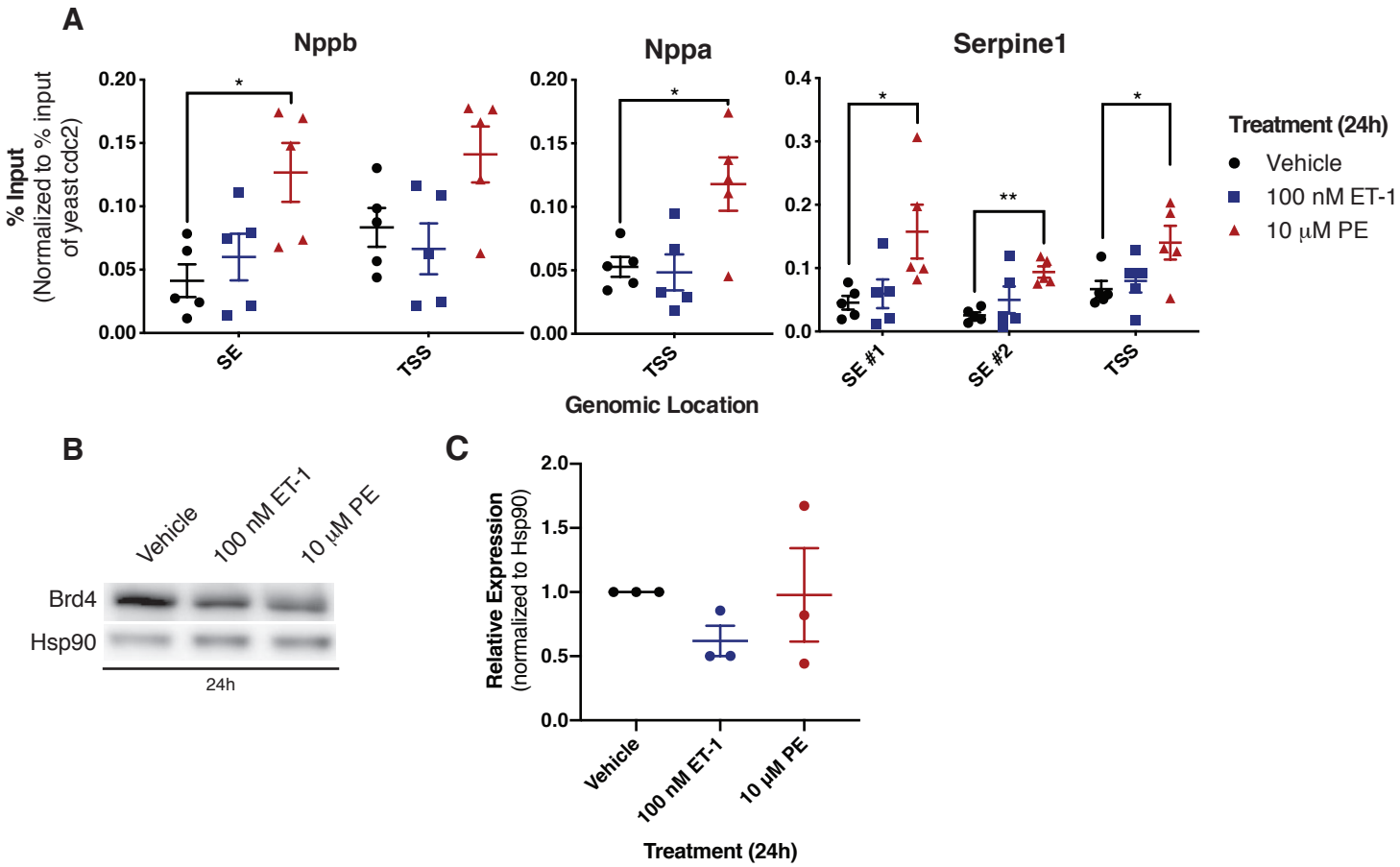

Figure 6. Brd4 chromatin occupancy increases in response to α_1-AR but not ETR activation. (A) Cardiomyocytes were treated for 24 h as indicated with DMSO (0.1%). Following treatment, crosslinked chromatin was immunoprecipitated with an anti-Brd4 antibody, followed by DNA purification and quantification by qPCR using primers at the indicated loci. Each immunoprecipitation was normalized to the % input for exogenous S. pombe spike-in DNA at the cdc2+ loci. Data was analyzed by one-way ANOVA followed by Dunnett's post-hoc comparison. (B) A western blot to assess changes in Brd4 protein expression following the indicated treatment for 24 h. (C) Densitometry based quantification of Brd4 normalized to Hsp90 expression. Data is presented as mean ± S.E.M with each point representing a biological replicate. Data was analyzed by one-way ANOVA followed Dunnett's post-hoc comparison (*p<0.05, **p<0.01).

Figure 7

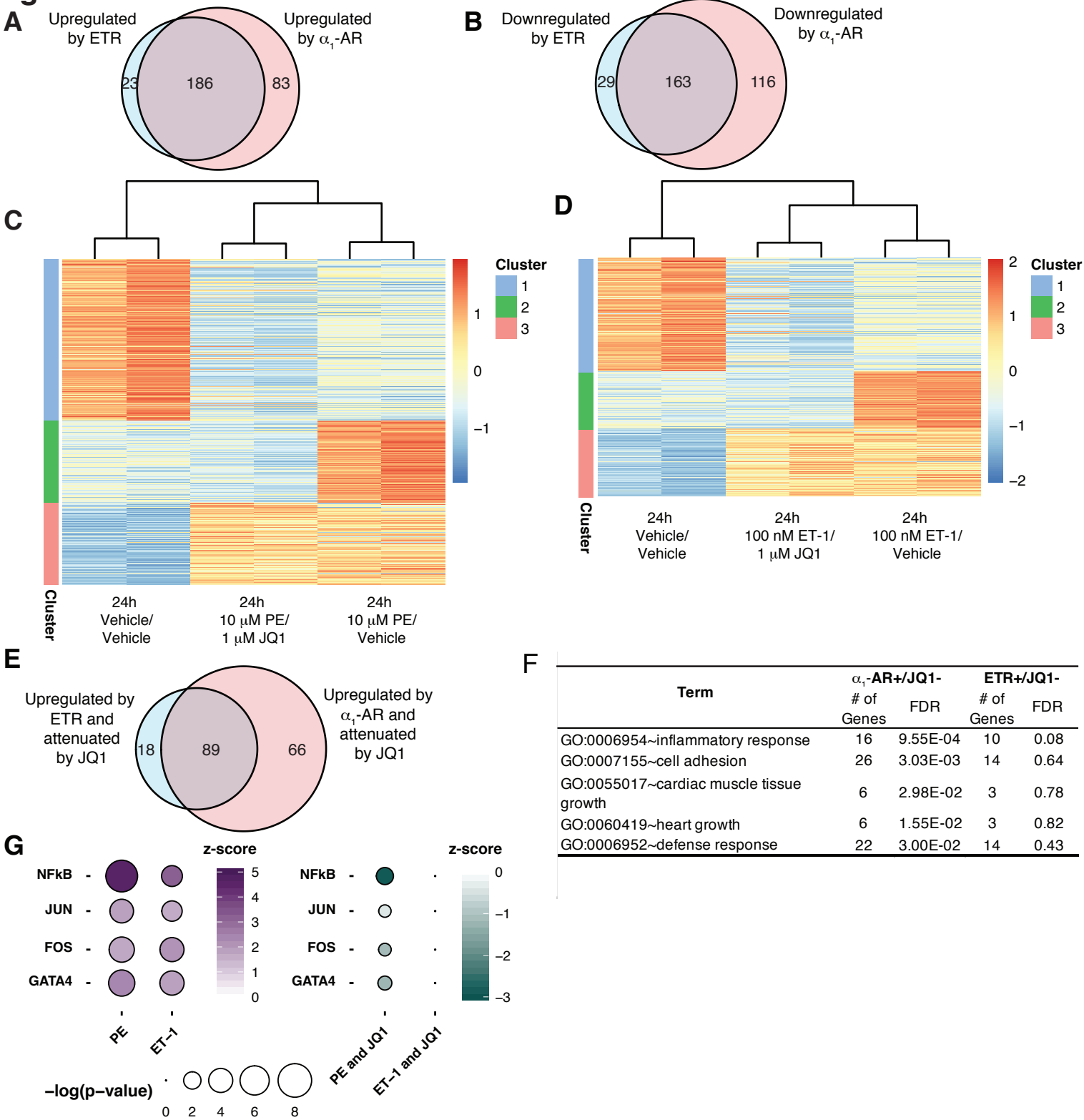

F

Term	α_1-AR+/JQ1- # of Genes	FDR	ETR+/JQ1- # of Genes	FDR
GO:0006954~inflammatory response	16	9.55E-04	10	0.08
GO:0007155~cell adhesion	26	3.03E-03	14	0.64
GO:0055017~cardiac muscle tissue growth	6	2.98E-02	3	0.78
GO:0060419~heart growth	6	1.55E-02	3	0.82
GO:0006952~defense response	22	3.00E-02	14	0.43

Figure 7. Transcriptome analysis of gene expression programs mediated by receptor activation and the effect of Brd4 inhibition. (A) Venn diagram of significantly upregulated genes (log2FC > 1 for Agonist/Vehicle vs Vehicle/Vehicle, p-value < 0.05) or (B) downregulated genes (log2FC < -1 for Agonist/Vehicle vs Vehicle/Vehicle, p-value < 0.05) following 24 h receptor activation. (C and D) Heat maps were generated for genes differentially regulated following activation of the specified receptor for 24 h. Each row was normalized, with the color representing the z-score for the specific row. K-means clustering was performed to identify subsets of genes with distinct patterns following Brd4 inhibition. (E) Venn diagram of genes upregulated by respective receptor activation (log2FC > 1 for Agonist/Vehicle vs Vehicle/Vehicle, p-value < 0.05) and attenuated by Brd4 inhibition from the activated state (log2FC < -0.5 for Agonist/JQ1 vs Agonist/Vehicle, p-value < 0.05). (F) Gene ontology enrichment for genes attenuated by JQ1 following receptor activation (from E) with DAVID. The false discovery rate (FDR) indicates whether the pathway was significantly enriched in the gene list. (G) Changes in transcription factor activity predicted by Ingenuity Pathway Analysis (IPA). The z-score represents the predicted change in transcription factor activity between the two compared treatment groups and the p-value indicates whether the transcription factor's targets are significantly enriched in the gene set. The purple dots (left side) indicate the change in activity following agonist treatment alone (log2FC > 1 for Agonist/Vehicle vs Vehicle/Vehicle, p-value < 0.05). The green dots (right side) indicate the JQ1 dependent decrease in activity from the activated state (log2FC < -0.5 for Agonist/JQ1 vs Agonist/Vehicle, p-value < 0.05).

Figure 8

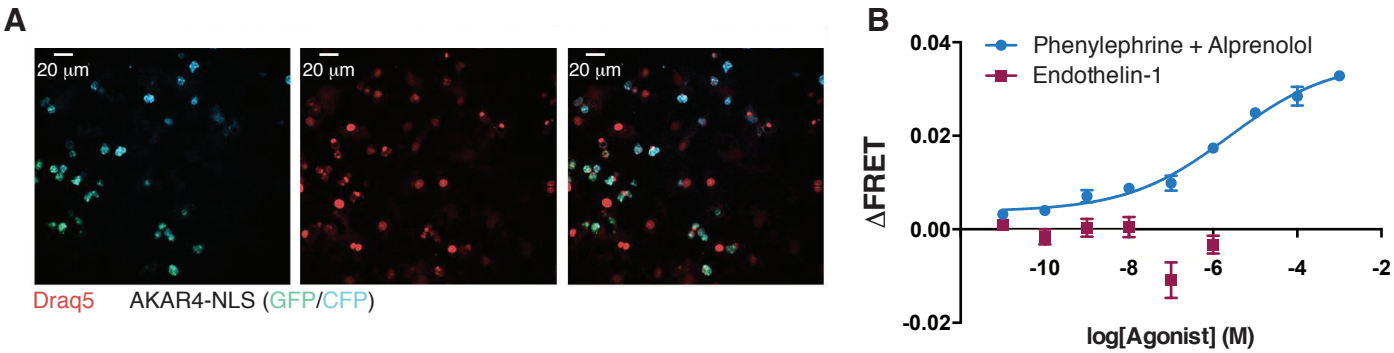

Figure 8. α_1-AR activation leads to increased nuclear PKA signalling. (A) Cardiomyocytes were transduced with AAV9-AKAR4-NLS virus at a MOI of 5000 and imaged 72 h later. Nuclei were visualized by staining live cells with Draq5. (B) Dose-response curves for PKA activation following activation of the ETR or α_1-AR were generated. Alprenolol was included to prevent off-target β-AR activation by high concentrations of PE. Data is presented mean ± S.E.M for three biological replicates. Dose response curves were plotted using sigmoidal dose response (variable slope) curves by non-linear regression.

Figure 9

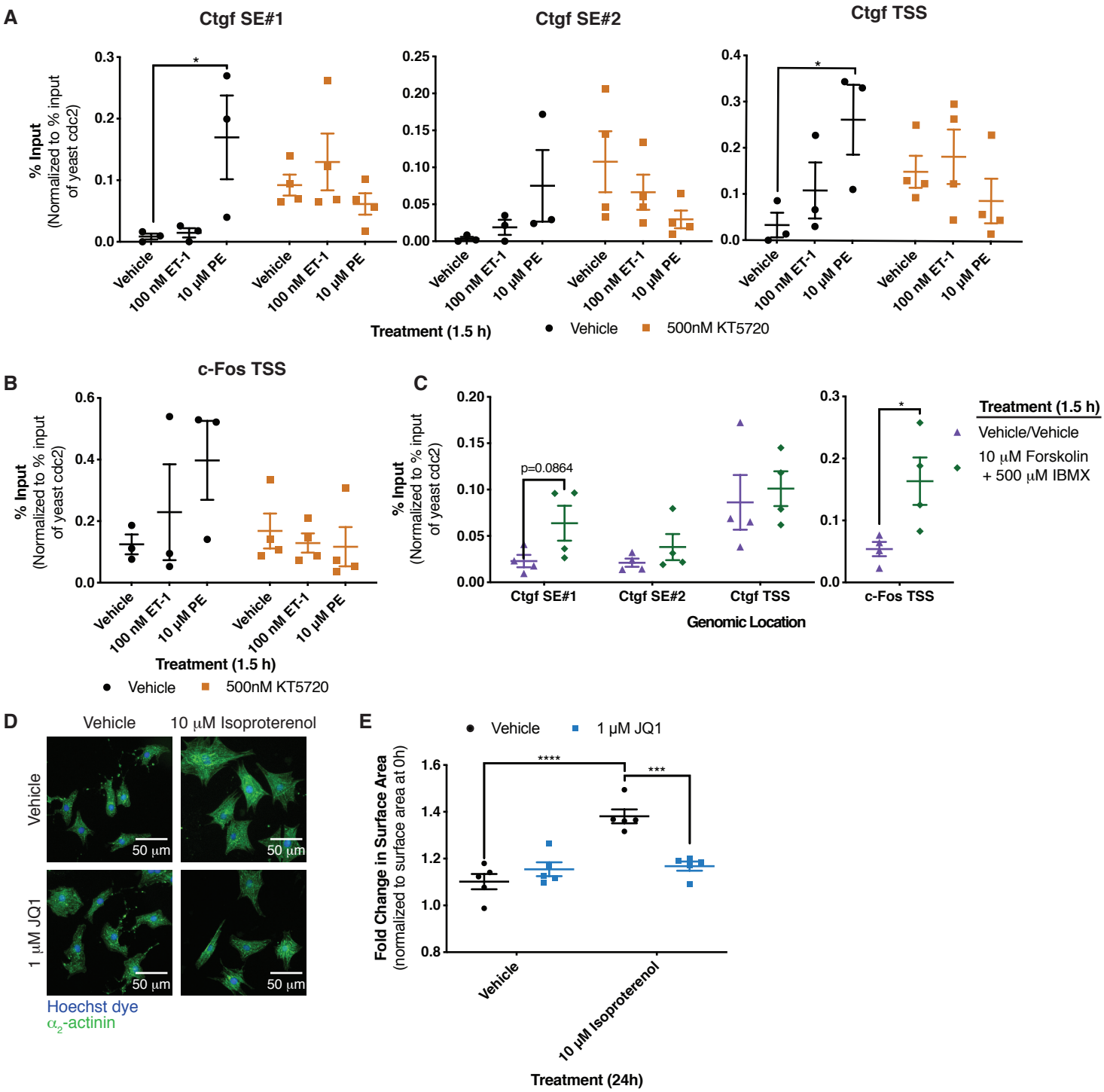

Figure 9. PKA signalling regulates recruitment of Brd4 to chromatin. (A and B) Effect of PKA inhibition with the small-molecule inhibitor KT5720 on receptor-mediated increases in Brd4 occupancy. Cardiomyocytes were pre-treated for 30 min with the PKA inhibitor prior to receptor activation for 1.5 h with the indicated agonists. Two-way ANOVA followed by post-hoc t-test comparisons with Bonferroni correction was performed. (C) PKA was activated for 1.5 h by increasing intracellular cAMP levels with forskolin and IBMX, an adenylyl cyclase activator and phosphodiesterase inhibitor respectively. Following indicated treatment, cardiomyocytes were fixed, and ChIP was performed with an anti-Brd4 antibody. ChIP was quantified by qPCR using primers at the indicated loci. An unpaired t-test was performed. (D) After 24 h of the indicated treatments, NRCMs were fixed and stained with Hoechst dye and for the cardiomyocyte specific marker α2-actinin. (E) Fold change in surface area after 24 h of the indicated treatment over cardiomyocytes fixed at 0 h from the same biological replicate. Two-way ANOVA followed by post-hoc t-test comparisons with Bonferroni correction was performed. Data is presented as mean ± S.E.M with each point representing a separate biological replicate. (*p<0.05, ***p<0.001, ****p<0.0001).

Figure 10

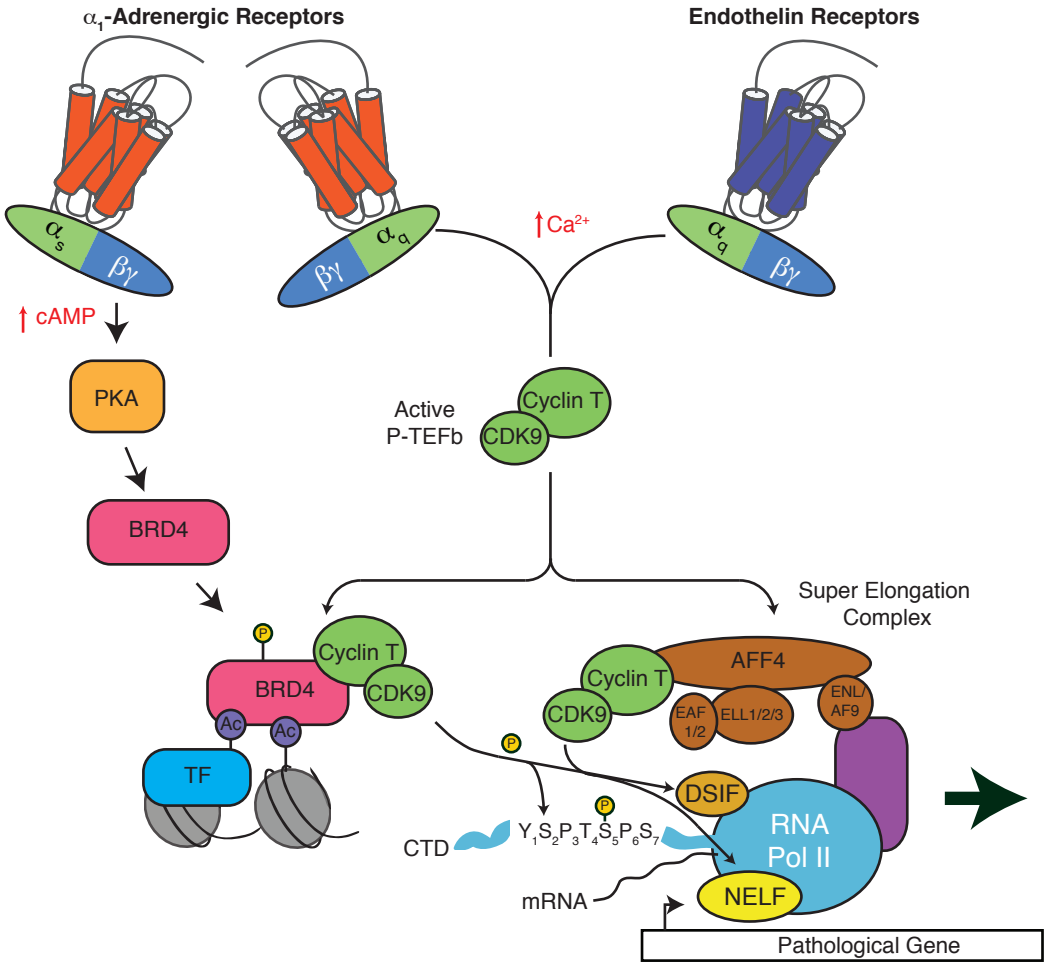

Figure 10. Model of P-TEFb complex activation following activation of the α_1-AR or ETR. Both the ETR and α_1-AR activate a signalling cascade which increases active P-TEFb and requires subsequent recruitment through the SEC. The α_1-AR activation also leads to Brd4-dependent recruitment due to the activation of a PKA signalling pathway.